AD

HDL-TM-70-18

MATHEMATICAL MODELING OF RESPIRATORY GAS EXCHANGE IN CAPILLARY TUBE OXYGENATORS WITH STEADY BLOOD FLOW

by

Fernando Villarroel

August 1970

U.S. ARMY MATERIEL COMMAND
HARRY DIAMOND LABORATORIES
WASHINGTON, D.C. 20438

92

The findings in this report are not to be construed as an official Department of the Army position, unless so designated by other authorized documents.

Destroy this report when it is no longer needed. Do not return it to the originator.

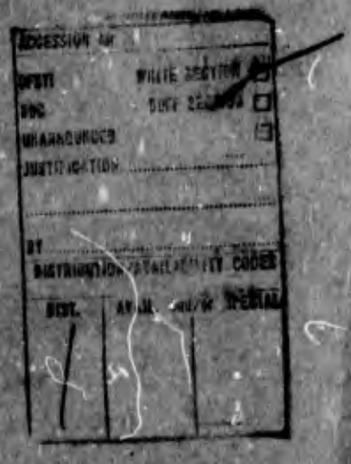

AD

DA-3AO62110A816.10
AMCMS Code: 5910.21.63232
HDL Proj: 31000

HDL-TM-70-18

MATHEMATICAL MODELING OF RESPIRATORY GAS EXCHANGE IN CAPILLARY TUBE OXYGENATORS WITH STEADY BLOOD FLOW

by

Fernando Villarroel

August 1970

U.S. ARMY MATERIEL COMMAND
HARRY DIAMOND LABORATORIES
WASHINGTON, D.C. 20438

ABSTRACT

A mathematical model for the transport of oxygen and carbon dioxide to blood flowing in semipermeable tubes under steady-flow conditions is presented. The model considers the membrane resistance to gas transport and allows for an additional interfacial resistance (protein deposition, etc). The possibility of gas transport augmentation due to rotation of erythrocytes in the velocity field is included in the model; however, no evidence of this augmentation was found in the flow range in which the model was compared with experimental data. The partial differential equation for the gas transport was solved numerically using a digital computer. Simultaneous solutions for oxygen and carbon dioxide were obtained, and the pH was computed for any point in the tube. Comparison of experimental data obtained by the author and other investigators with the curves predicted by the model shows excellent agreement. The numerical solution of the transport equation yields the bulk average values of pH, carbon dioxide partial pressure, and oxygen saturation, as well as the internal value of these parameters as a function of tube length and radius. A simple steady flow design equation, which is a reasonable approximation of the computer results for a wide range of venous blood conditions, is presented.

TABLE OF CONTENTS

TABLES

TABLE OF CONTENTS (Cont'd)

TABLES (Cont'd) Page No.

ILLUSTRATIONS

Figure

ILLUSTRATIONS (Cont'd)

Figure — Page No.

1. INTRODUCTION

The use of extracorporeal gas exchangers for the oxygenation of blood and removal of carbon dioxide during surgical lung bypass is an established practice today (ref 1). The early devices were simple in concept and operation—the exchange of gases was generally made through a direct gas-blood interface, either through bubbles or thin films. This exchange mechanism has a high efficiency, and these devices proved the feasibility of the extracorporeal exchange of respiratory gases. The major limitations to their use for long term perfusion are imposed by the irreversible damage to various blood constituents caused by mechanical trauma and direct blood-gas interfacing.

Recent efforts attempt to reduce mechanical shear stress by using better materials and fewer moving parts, and to reduce the liquid surface stress. The introduction of a semipermeable membrane between the gas and liquid faces appears to accomplish both objectives. This report presents a mathematical model of the gas transport in a semi-permeable capillary-tube gas exchanger through which the blood is flowing steadily. This problem has been analyzed by other investigators—particularly, by Buckles (ref 2) and Weissman and Mockros (ref 3). The theories developed by these investigators do not fully agree with existing data or do not consider all the parameters involved in the gas transport. The solution proposed in this report is more general or complete than those previously developed. The solutions of the differential equations for oxygen and carbon dioxide are obtained simultaneously, and the pH is computed for any point of the tube. Internal concentration profiles for both gases and pH internal profile are obtained as a function of the radius and length of the tube. Comparison of the solution with the data obtained by other investigators (ref 2,3) and the data compiled herein shows excellent agreement.

2. LITERATURE SURVEY

The mathematical analysis and modeling of the steady-state flow capillary tube blood gas exchangers, normally called oxygenators, has been attempted by earlier investigators with varying degrees of success. Marx, et al (ref 4) developed a model describing the transient phenomenon of oxygenation of blood films, where the oxygen path is several times the order of magnitude of the diameter of the red cells. Bradley and Pike (ref 5) studied the gas transport in capillary tubes. But the work of Buckles (ref 2)--later published by Buckles, Merrill, and Gilliland(ref 6)—and the papers published by Weissman and Mockros (ref 3) and Thews (ref 7) are indeed the most important papers published in this field.

The model developed by Weissman and Mockros is very similar to the model developed earlier by Buckles. Buckles' steady-state oxygen

transport differential equation, properly transformed to the symbols used elsewhere in this paper, is given below

$$\frac{D_o}{r}\frac{\partial}{\partial r}\left\{r\frac{\partial C}{\partial r}\right\} = V_z\left\{\frac{\partial C}{\partial Z} + \frac{\partial s}{\partial Z}\right\}, \qquad (1)*$$

where the oxygen content of the sinks (RBC), s, is a function of the gas concentration C. The term $\partial s/\partial Z$ at constant pH can be written as

$$\frac{\partial s}{\partial Z} = \frac{ds}{dC}\frac{\partial C}{\partial Z} \quad . \qquad (2)$$

Substituting equation (2) into (1), the following equation is obtained

$$\frac{D_o}{r}\frac{\partial}{\partial r}\left\{r\frac{\partial C}{\partial r}\right\} = V_z\left\{1 + \frac{ds}{dC}\right\}\frac{\partial C}{\partial Z} \quad . \qquad (3)$$

This differential equation is the same equation obtained by Weissman and Mockros (ref 3), using the substantial derivative to describe the rate at which the oxygen is delivered or absorbed by the sinks.

The numerical solutions to equation 3 obtained by these investigators differ mainly in the boundary conditions and in the numerical method used. Buckles did a full analysis of the gas transport through the wall and considered the wall flux as one of the boundary conditions. He numerically solved the transport differential equation (3), using the Crank-Nicolson method. Weissman and Mockros ignored the effect of the wall on the overall gas transport and assumed that the partial pressure of the gas at the wall-blood interface was constant and equal to the partial pressure of the gas outside the wall. The gas transport differential equation was solved numerically by Weissman and Mockros, using straightforward finite differences techniques rather than the Crank-Nicolson method. These researchers obtained the value of the diffusivity D_o by fitting their numerical results to their own experimental data and using D_o as an independent parameter. The value of the diffusivity determined in this way is inaccurate, since it is affected by the wall characteristics not considered by the model.

Another, perhaps less important, difference between the two models is the shape of the velocity profile. Buckles used the Casson (ref 8) model, whereas Weissman and Mockros used a simple Newtonian parabolic model. However, the Casson model approximates a parabolic profile in the flow range of the data taken by these investigators. The theoretical curve developed by Buckles (ref 2) and experimental data he obtained using whole fresh human blood are shown in figure 1. The graph shows that the theoretical prediction is reasonable at high flows, but it is

*Nomenclature of symbols listed on pp. 69 - 72.

too low in the low-flow region. For example, at flows of the order of 0.1 cc/min, the theoretical curve is 30 to 45 percent lower than that for the actual laboratory data.

Buckles' (ref 2) work, in this author's opinion, is an excellent analysis of the oxygenation phenomenon in flowing blood under steady-flow conditions. However, the comparison between his data obtained under carefully controlled conditions and his theoretical prediction shows a considerable discrepancy. Preliminary explanations for this discrepancy include facilitated oxygen transport either by hemoglobin diffusion and/or rotation of the red cells in the velocity field. The mechanism of facilitated oxygen transport by hemoglobin diffusion was first shown by Schollander (ref 9). Roughton (ref 10) suggested, however, that this phenomenon does not occur in the red cells because of the high concentration of hemoglobin. When the concentration of hemoglobin is high, the molecules act as closely packed spheres (ref 11,12) and diffusion of the molecules is not likely to occur. Klug, et al (ref 13) measured the diffusivity of oxygen in hemoglobin solutions and found that at concentrations similar to those of the human red cells (about 35-g percent), the augmentation effect was negligible. Diffusion augmentation due to rotation of the red cells (ref 14) has been included in the model developed in this paper and found to be unimportant. A reasonable explanation lies in the numerical solution employed. The solution to the equations employing a finite difference algorithm used in this study greatly improves the fit of the model's prediction with Buckles' data, as described and illustrated in section 4.2.

A different modeling of the gas transport in whole blood is the moving front concept of Thews (ref 7). The blood is considered as two concentric regions separated by a moving front. The region next to the tube wall is assumed to be saturated while the one close to the tube axis is reduced. Diffusion takes place through the saturated annular region to the interface between the two regions where the oxygen reacts with the hemoglobin. This model is simpler but does not accurately describe the actual physical phenomenon of gas transport in flowing blood. Theoretical internal profile curves, presented later in this paper, will show perhaps a more realistic picture of the blood behavior. Buckles (ref 2) compared Thew's model with experimental data and with his own model, and showed that the advancing front theory is not conservative but, instead, predicts saturations higher than either the experimentally measured ones or the saturations computed using his theory.

Several other investigators studied systems that are closely related to the system described in the report. Among them are Keller and Friedlander (ref 15) who studied the steady-state transport of oxygen through hemoglobin solutions; Spaeth and Friedlander (ref 16) who studied gas transfer in a rotating disk boundary layer flow; and

Lightfoot (ref 17) who developed a low-order approximation for membrane blood oxygenators. Jones (ref 18), Merrill, et al (ref 19), and Dorson and Hershey (ref 20) studied the hydrodynamic behavior of blood flowing in capillary tubes.

3. MATHEMATICAL MODEL

3.1 Basic Assumptions

Consider the problem of blood flowing at a steady rate inside a semipermeable tube of constant diameter exposed to an oxygen rich atmosphere. As the blood flows through the tube, oxygen diffuses radially into the blood, and carbon dioxide follows the opposite path. At the same time, the erythrocytes act as reversible gas sinks absorbing oxygen and giving up carbon dioxide. The assumptions used in describing the model are:

(a) The axial diffusion through the wall is negligible.
(b) The system is isothermal.
(c) The blood is a homogeneous, incompressible, non-Newtonian fluid where the velocity profile is described by an integrated form of the Casson (ref 8) equation. This assumption implies that:
    1. The velocity vector is parallel to the tube wall,
    2. The velocity of the blood at the wall is zero, and
    3. There is no red cell migration.
(d) At any point, the gas contained in the sinks is in equilibrium with the gas dissolved in the adjacent plasma--
    1. The gas-sink reaction is instantaneous, and
    2. The sinks are homogeneously distributed in the fluid.
(e) Axial gas transport by diffusion in the blood is negligible compared with the gas transport due to blood flow.
(f) The oxygen consumed by metabolic process during oxygenation of the test blood is negligible.

3.2 Gas Mass Balance

The differential equation describing the gas concentration distribution will be obtained, making a mass balance for the gas over an annular element of fluid. The element of fluid is shown in figure 2. Gases enter and leave this element by diffusion and by fluid flow. The contributions to the mass balance are listed below.

Gas in by diffusion at r $\quad r\, n_r|_r\, 2\pi\, \Delta Z$

Gas out by diffusion at r+Δr $\quad r\, n_r|_{r+\Delta r}\, 2\pi\, \Delta Z$

Gas in by flowing fluid at Z	$C\|_z \; V_z \; 2\pi \; r \; \Delta r$
Gas out by flowing fluid at Z+ΔZ	$C\|_{z+\Delta z} \; V_z \; 2\pi \; r \; \Delta r$
Apparent gas reaction rate of the fluid element	$S \; 2\pi r \; \Delta r \; \Delta Z$

where S is the apparent gas reaction rate per unit volume. The apparent gas reaction rate is defined as the moles of gas delivered or absorbed by the gas sinks contained in the element of fluid, per unit time, due to the displacement of this element from one coordinate to the next.

For steady-state conditions, the mass balance is described by the following relation.

$$\begin{bmatrix}\text{rate of mass}\\ \text{out}\end{bmatrix} - \begin{bmatrix}\text{rate of mass}\\ \text{in}\end{bmatrix} + \begin{bmatrix}\text{rate of mass}\\ \text{disappearance}\\ \text{by reaction}\end{bmatrix} = 0$$

Substituting each variable by its mathematical expression yields

$$\frac{r\, n_r|_{r+\Delta r} - r\, n_r|_r}{\Delta r} + r\, V_z \frac{C|_{z+\Delta z} - C|_z}{\Delta Z} + S\, r = 0 \qquad (4)$$

Taking the limit of equation (4) as $\Delta r \to 0$ and $\Delta Z \to 0$ yields

$$\frac{\partial (r\, n_r)}{\partial r} + r\, V_z \frac{\partial C}{\partial Z} + S\, r = 0. \qquad (5)$$

The molar flux is related to the concentration gradient by Fick's law

$$n_r = -D \frac{\partial C}{\partial r} \quad , \qquad (6)$$

where D is the effective diffusivity considering the augmentation effect. The resulting differential equation after substituting equation (6) in (5) is

$$\frac{1}{r} \frac{\partial}{\partial r} \left\{ r\, D \frac{\partial C}{\partial r} \right\} = V_z \frac{\partial C}{\partial Z} + S \qquad (7)$$

This equation can be solved if the values of S, V_z, and D are defined. The following sections are devoted to the definition of these parameters.

3.3 Apparent Reaction Rate

The oxygen or carbon dioxide stored in the sinks, s, is in equilibrium with the gas dissolved in the plasma but does not contribute

to the gas partial pressure. Under steady-state conditions, the rate at which the gas is stored or delivered by the sinks per unit volume of blood, S, is given by the substantial derivative of s,

$$S = \frac{Ds}{Dt} \quad . \tag{8}$$

Rearranging equation (8) yields

$$S = \frac{ds}{dC} \frac{DC}{Dt} \quad . \tag{9}$$

where the substantial derivative of the concentration is given by

$$\frac{DC}{Dt} = \frac{\partial C}{\partial t} + V_r \frac{\partial C}{\partial r} + \frac{V_\theta}{r} \frac{\partial C}{\partial \theta} + V_z \frac{\partial C}{\partial Z} \quad , \tag{10}$$

However, at steady state

$$\frac{\partial C}{\partial t} = 0 \text{ and by previous assumption } V_r = 0;\ V_\theta = 0 \tag{11}$$

thus, the substantial derivative becomes

$$\frac{DC}{Dt} = V_z \frac{\partial C}{\partial Z} \quad . \tag{12}$$

Substituting equation (12) into (9) yields

$$S = \frac{ds}{dC} V_z \frac{\partial C}{\partial Z} \quad . \tag{13}$$

Equation (13) describes the reaction rate S per unit volume of blood.

The total oxygen content of a unit volume of blood is given by the oxygen dissociation curve shown in figure 3 (ref 21) and described in detail in appendix A. This curve closely represents the oxygen stored in the red cells since the oxygen dissolved in the plasma is comparatively very small. Defining T as the g-moles of oxygen stored in the red cells per liter of blood when the red cells are fully saturated, the oxygen dissociation curve gives the percent, PS, of the maximum saturation, T, versus the partial pressure of oxygen in mm Hg. For normal blood, assuming a hemoglobin concentration of 15-g percent (g/100 cc of blood), T is $9.1\ 10^{-3}$ g-mole/liter. Thus, the oxygen stored per unit volume of blood in g-mole/liter, s, is

$$s = \frac{T}{100} PS \quad . \tag{14}$$

The relationship between the carbon dioxide stored in the sinks per unit volume of blood and the carbon dioxide partial pressure considering the Haldane effect is given by the following equation(ref 22),

which is a good approximation for most of the partial pressure range

$$s = 1.14\ 10^{-2} + 2.51\ 10^{-4}\ pCO_2 \quad , \tag{15}$$

where the pCO_2 is given in mm Hg and the stored carbon dioxide in g-mole/liter.

The carbon dioxide partial pressure in mm Hg is related to the concentration of carbon dioxide in the plasma in g-mole/liter by the following relationship (ref 22)

$$pCO_2 = 3.59\ 10^4\ C. \tag{16}$$

Substituting equation (16) into equation (15) yields

$$s = 1.14\ 10^{-2} + 9.0\ C\ . \tag{17}$$

From equations (14) and (17), the value of ds/dC is

$$\frac{ds}{dC} = \frac{T}{100}\ \frac{d}{dC}(PS) \quad \text{for oxygen, and} \tag{18}$$

$$\frac{ds}{dC} = 9.0 \quad \text{for carbon dioxide} \tag{19}$$

The function PS is given in appendix A.

3.4 Velocity Profile

The non-Newtonian behavior of blood has been extensively investigated under steady-flow conditions. The constitutive relation used in this paper is that obtained by Casson (ref 8) for the flow of printing ink. Merrill, et al (ref 19), showed that the Casson relation represents the non-Newtonian behavior of blood within reasonable accuracy. The Casson equation is expressed as

$$\tau^{1/2} = \tau_o^{1/2} + \left\{-\eta\ \frac{dV_z}{dr}\right\}^{1/2} \tag{20}$$

Substituting the Casson relation into the equation of motion for the shear stress and using the boundary conditions,

$$V_z = 0 \quad \text{at } r = R$$

$$\frac{dV_z}{dr} = 0 \quad \text{at } r = r_o\ .$$

Where r_o is the radius of the plug flow region, the following relationships for the axial velocity are obtained.

For $r^* > \gamma$

$$V_z = \frac{R\,\tau_o}{2\,\gamma\,\eta}\{1 - (r^*)^2 - (8/3)\,\gamma^{1/2}\,[1 - (r^*)^{3/2}] + 2\gamma(1 - r^*)\} \quad (21)$$

and for $r^* < \gamma$

$$V_z = \frac{R\,\tau_o}{2\,\gamma\,\eta}\{1 + 2\,\gamma - \gamma^{2/3} - (8/3)\,\gamma^{1/2}\} \quad (22)$$

where $r^* = r/R$ and $\gamma = r_o/R$.

The volumetric flow, Q, is given by

$$Q = \frac{\pi R^3}{4\,\gamma\,\eta}\{1 - (16/7)\,\gamma^{1/2} + (4/3)\,\gamma - (1/21)\,\gamma^4\} \quad (23)$$

The details of the solution are given in appendix B. The parameters η and τ_o were determined, using the data obtained by Dorson and Hershey (ref 20).

Figure 4 is a plot of these data for three tube diameters, and the theoretical relation obtained from equation 23 using $\tau_o = 0.07$ dynes/cm^2 and $\eta = 0.0283$ poises. The dimensionless velocity profile as a function of the dimensionless radius for $\gamma = 0$ and $\gamma = 0.5$ is shown in figure 5.

3.5 Diffusivity

The flux of a chemical species from a region of high concentration to a region of low concentration is described by Fick's law, which essentially establishes that the flux is proportional to the concentration gradient. The proportionality parameter, called diffusivity, may be either a constant or a function of other variables. In the case of the transport of gases in blood, the flux may be described by the sum of two terms: the ordinary diffusion flux and a flux introduced by the rotation of the erythrocytes in the velocity field. If the second flux is somehow proportional to the concentration gradient, the total effective diffusivity becomes the sum of the ordinary diffusivity D_o and the proportionality term between the rotation-induced flux (or augmented flux) and the concentration gradient which may be called rotation-induced diffusivity D_{rot}. The effective diffusivity becomes then

$$D = D_o + D_{rot} \quad (24)$$

The following two sections will be devoted to the definition of D_o and D_{rot}.

3.5.1 Augmented Diffusion

The possibility of augmented diffusion in flowing blood has been reported in the literature (ref 14). Particles suspended in shear flow rotate as they move along with the fluid. Their velocity of rotation is a function of the shear rate of the fluid and of the particle shape and rigidity (ref 23). The rotating particles introduce a local radial component of velocity with a resulting mixing effect that can be expressed as an augmented diffusion. The actual complexities of this phenomenon prevent its exact mathematical description; however, the problem can be approched using an analysis similar to that used in developing the Prandtl mixing-length theory. Keller and Leonard (ref 14), based on the theory presented by Goldsmith and Mason (ref 23), obtained an expression for the rotation-induced flux around rotating spheres and assumed that the resulting relation also predicts the flux around tumbling red cells

$$n_{rot} = \left\{ \frac{\delta^2}{8} \frac{dV_z}{dr} \right\} \frac{\partial C}{\partial r} \qquad (25)$$

where δ is the diameter of the red cell. However, if this flux is to be used in conjunction with the ordinary flux, it should be averaged over the whole volume occupied by the red cell and its corresponding surrounding fluid. The average rotation-induced gas flux is then

$$n_{rot} = \left\{ \varphi \frac{\delta^2}{8} \frac{dV_z}{dr} \right\} \frac{\partial C}{\partial r} \quad , \qquad (26)$$

where φ is an unknown factor generally dependent on hematocrit, erythrocyte volume, and boundary layer thickness around the erythrocyte. Expressing this flux as the result of augmented diffusion, the rotation-induced diffusivity is

$$D_{rot} = - \beta \frac{dV_z}{dr} \quad , \qquad (27)$$

where $\beta = \varphi \delta^2/8$ is called the blood-mixing coefficient in analogy to the mixing length in Prandtl theory. β is unknown and should be experimentally determined.

3.5.2 Ordinary Diffusivity in Whole Blood

Ordinary diffusivity of oxygen in whole blood and in hemoglobin solutions have been reported by several investigators—among them, Hershey and Karhan (ref 24) who measured oxygen diffusivity in fully saturated sheep blood over a wide range of hematocrits; Keller and Friedlander (ref 15) who studied the steady-state transport of oxygen through hemoglobin solutions; and Klug (ref 13) who investigated the oxygen diffusivity in hemoglobin solutions.

Assuming that the red cell membrane does not offer significant resistance to the oxygen transport as suggested by Thews (ref 25)and Kreuzer and Yahr (ref 26), the blood can be idealized as pure plasma with discrete regions of red cell cytoplasma with no interfacial resistance. The red cell cytoplasma may be considered as a concentrated solution of hemoglobin with a diffusivity of $D_{rbc} = 0.35\ 10^{-6}$ cm^2/sec (ref 13 for a hemoglobin concentration of 35.5-g percent). The average value of the diffusivity of pure plasma (ref 13, 24) appears to be $D_p = 1.99\ 10^{-5}$ cm^2/sec. Applying the theoretical equation obtained by Fricke (ref 27) for the electrical conductivity of heterogeneous suspensions to this model and substituting the electrical conductivities by the diffusivities, the following equation can be established.

$$\frac{\left\{\frac{D_o}{D_p} - 1\right\}}{\left\{\frac{D_o}{D_p} - X\right\}} = \frac{\left\{\frac{H}{100}\right\}\left\{\frac{D_{rbc}}{D_p} - 1\right\}}{\left\{\frac{D_{rbc}}{D_p} + X\right\}}, \qquad (28)$$

where X is a parameter dependent on the ratio D_{rbc}/D_p and the geometrical characteristics of the erythrocyte. Fricke (ref 27) developed this equation for ellipsoidal particles and assumed that the behavior of the red cells could be represented by his model. He determined that the ratio of the axes of the ellipsoidal particles representing the red cells is 0.235. Using this ratio and the ratio $D_{rbc}/D_p = 0.175$, together with the chart developed by Fricke (ref 27), the value of the parameter X becomes 1.22. Substituting the numerical values into equation (28) and rearranging yields

$$D_o = 1.99\ 10^{-5}\ \frac{100 - 0.727\ H}{100 + 0.591\ H} \qquad (29)$$

Equation (29) is plotted in figure 6.

The value of the diffusivity of carbon dioxide in blood was estimated, using an analogy with pure water. For pure water (ref 28)

$$\frac{\text{Carbon dioxide diffusivity}}{\text{Oxygen diffusivity}} = 0.9833 .$$

This ratio was assumed to be the same for whole blood.

3.6 Transport Equation

Equation (7) is the general transport equation in which the apparent reaction rate S, the fluid velocity V_z, and the diffusivity D are unknowns. The reaction rate is given by equations (13), (18) and (19); the fluid velocity is described by equations (21) and (22); and the diffusivity is given by equations (24), (27), and (29). Substituting these equations into equation (7), the following differential equation is obtained.

$$\frac{F_2 + N_F F_1^2}{r^*}\left\{\left[F_2 + \frac{N_F F_1}{F_2 + N_F F_1^2} r^{*1/2}\right]\frac{\partial C}{\partial r^*} + r^* \frac{\partial^2 C}{\partial r^{*2}}\right\} = F F_3 \frac{\partial C}{\partial Z^*} , \qquad (30)$$

where

$$N_F = \frac{\tau_o \beta}{\gamma \eta D_o}$$

$$r^* = r/R$$

$$Z^* = \frac{2 \gamma \eta D_o Z}{\tau_o R^3}$$

$$\gamma = r_o/R$$

For $r^* > \gamma$,

$$F_1 = (r^*)^{1/2} - \gamma^{1/2}$$

$$F = 1 - (r^*)^2 - (8/3)\ \gamma^{1/2}\ [1 - (r^*)^{3/2}] + 2\gamma\ (1 - r^*) .$$

For $r^* < \gamma$,

$$F_1 = 0$$

$$F = 1 + 2\gamma - \gamma^2 / 3 - (8/3)\ \gamma^{1/2} .$$

For oxygen,

$$F_3 = 1 + \frac{T}{100} \frac{dPS}{dC}$$

$$F_2 = 1.0$$

For carbon dioxide,

$$F_3 = 10.0$$

$$F_2 = 0.9833$$

3.7 Boundary Conditions

The integration or numerical solution of equation (30) requires a set of boundary conditions—that is, statements of physical facts at specified values of the independent variables. The boundary conditions used in this paper for solving the transport equation are:

(a) The concentrations of oxygen and carbon dioxide are uniform and constant at the entrance of the tubes

$$C(r^*, 0) = C_o \quad , \tag{31}$$

where C_o has a different value for oxygen and for carbon dioxide.

(b) The radial mass flux at the center of the tube is zero for oxygen and for carbon dioxide

$$\frac{\partial}{\partial r^*}\{C(0, Z^*)\} = 0 \quad . \tag{32}$$

(c) The last boundary condition defines the gas transport through the wall. (Details of the derivation of this equation are given in appendix C.)

$$D \frac{\partial}{\partial r^*}\{C(1 , Z^*)\} = F_4 \frac{D_w}{1 \text{ OR}^*}[C_\infty - C(1 , Z^*)] \quad , \tag{33}$$

where F_4 expresses the interfacial resistance between the blood and the wall (protein deposition, etc), and C_∞ is the constant equivalent concentration defined as a hypothetical gas concentration in plasma corresponding to the outside partial pressure of the gas. The diffusivity of the gas in the wall is also expressed as equivalent diffusivity $D_w = D_m c_m / c_p$, where c_m and c_p are the gas solubilities in the membrane and in the plasma, and D_m is the gas diffusivity in the membrane.

3.8 Relation Between Carbon Dioxide Concentration and pH

The ratio of the concentration of bicarbonate to the concentration of carbon dioxide is the single most important factor in determining the pH of the blood. The chemical equilibrium equation determining

the existence of these species in solution in the plasma is

$$CO_2 + 2H_2O \rightleftarrows H_3O^+ + HCO_3^- \tag{34}$$

and the equilibrium among the species is given by

$$\frac{[H_3O^+]\ [HCO_3^-]}{[CO_2]} = 10^{-6.11} \tag{35}$$

Considering that $-\log[H_3O^+] = pH$, equation (35) can be rearranged to

$$pH = 6.11 + \log \frac{[HCO_3^-]}{[CO_2]} \quad , \tag{36}$$

the equation known as the Henderson-Hasselbach relation. From equation (35) it is also possible to show that

$$[HCO_3^-] = 10^{pH-6.11}[CO_2] \quad . \tag{37}$$

Su tuting equation (16) into equation (37) yields

$$[HCO_3^-] = \frac{pCO_2}{3.59\ 10^4}\ 10^{pH-6.11} \quad . \tag{38}$$

The stoichiometry of equation (34) shows that any change in oncentration of bicarbonate must be equal to the change in the ntration of hydronium,

$$\Delta[HCO_3^-] = \Delta[H_3O^+] = 10^{-pH_i} - 10^{-pH} \quad , \tag{39}$$

e pH_i is the initial value of the pH.

The percent of change in the bicarbonate concentration is given by

$$\frac{100\ \Delta[HCO_3^-]}{[HCO_3^-]} = \frac{3.59}{pCO_2}\ 10^{-(2\ pH\ -\ 12.11)}\ (10^{pH\ -\ pH_i} - 1). \tag{40}$$

For the extreme conditions pCO_2 = 1 mm Hg, pH_i = 5 and pH = 9, the percent of change in the bicarbonate concentration computed by using equation (40) is only 0.046 percent. This numerical value shows that the bicarbonate concentration can be assumed constant for computation of pH inside the gas exchanger tube; then

$$pH = 6.11 + \log\left\{\frac{\text{constant}}{[CO_2]}\right\} \quad , \tag{41}$$

where the constant can be computed from the initial conditions at the entrance of the tube.

3.9 Numerical Solution

A computer program (appendix D) was developed for a simultaneous solution of the oxygen and carbon dioxide differential equations. For a given set of boundary conditions, the program computes the concentration of oxygen and carbon dioxide, and the pH for points distributed in both the axial and the radial direction. The program also computes the cross-sectional average value of these parameters and the percent of oxygen saturation for points along the tube.

To execute the numerical solution on the digital computer, equation (30) was approximated by a finite difference equation in which the first derivative was replaced by the first forward difference, and the second derivative was replaced by the second forward difference. The oxygen dissociation curve, shown in figure 2, was curve fitted in three sections. The curve-fitting equations are given in appendix A. The oxygen percent of saturation PS and the apparent reaction rate S were computed, using these equations in the subroutine COSA. The dimensionless radius γ of the plug-flow region was computed in the subroutine GAMM using equation (23).

4. RESULTS AND DISCUSSION

4.1 Effect of Velocity Profile

Equation (23) may be rearranged to the following forms:

$$\frac{Q}{R^3} = \frac{\pi \tau_o}{4 \gamma \eta}\left\{1 - (16/7)\ \gamma^{1/2} + (4/3)\ \gamma - (1/21)\ \gamma^4\right\} \qquad (42)$$

and

$$\frac{\tau_o}{\gamma} = \frac{4 Q \eta}{\pi R^3}\left\{1 - (16/7)\ \gamma^{1/2} + (4/3)\ \gamma - (1/21)\ \gamma^4\right\}^{-1} \qquad (43)$$

Substituting equation (43) into (21) yields

$$V_z = \frac{2 Q}{\pi R^2} \frac{\left[1 - (r^*)^2\right] - (8/3)\ \gamma^{1/2}\left[1 - (r^*)^{3/2}\right] + 2\gamma\ (1 - r^*)}{1 - (16/7)\ \gamma^{1/2} + (4/3)\ \gamma - (1/21)\ \gamma^4} \qquad (44)$$

On the other hand, for a Newtonian fluid, the velocity profile is given by

$$V_z = \frac{2 Q}{\pi R^2}\left[1 - (r^*)^2\right] \ . \qquad (45)$$

Table I shows a comparison between the velocity profile given by a Newtonian fluid and that given by equation (44), taking an arbitrary value of $\gamma = 0.01$; that is, the plug-flow region is 1 percent of the tube radius.

The values of the dimensionless velocities given in table II show that when the plug-flow region becomes 1 percent or less of the tube radius, the velocity profile can be safely assumed to be parabolic.

Substitution of the numerical values of τ_o, η, and $\gamma = 0.1$ in equation (42) gives $Q/R^3 = 192\ \text{sec}^{-1}$. This result shows that for Q/R^3 larger than $192\ \text{sec}^{-1}$, the velocity profile can be assumed to be parabolic and the blood can be treated as Newtonian fluid.

Substitution of the value of τ_o/γ from equation (43) into the definition of N_F and Z^* given under equation (30) gives the following simpler expressions for these parameters

$$N_F = \frac{4\ Q\ \beta}{\pi\ R^3\ D_o} \tag{46}$$

$$Z^* = \frac{\pi\ D_o\ Z}{2\ Q} \tag{47}$$

When the velocity profile is parabolic ($Q/R^3 > 192\ \text{sec}^{-1}$), the transport differential equation (30) together with equations (46) and (47) show that if the dimensionless blood mixing coefficient N_F is assumed zero, the equation becomes explicit in R. Hence, the radially averaged concentration over r* can be expressed as a function of Z* alone.

Table I. Comparison between Parabolic Velocity Profile and Casson Velocity Profile for $\gamma = 0.1$

r*	$V_z/(2Q/\pi R^2)$		Percent error
	Parabolic	Casson	
0	1.0000	1.0000	0
0.2	0.9600	0.9609	+0.09
0.4	0.8400	0.8402	+0.02
0.6	0.6400	0.6398	-0.03
0.8	0.3600	0.3599	-0.03
1.0	0	0	0

4.2 Comparison with Buckles' Experimental Data and Theoretical Results

The experimental results obtained by Buckles (ref 2,6) using fresh human blood are tabulated in table II. He carefully determined the oxygen dissociation curve of the blood donated for his experiment. The curve determined by Buckles at a pH of 7.14 coincides with the standard curve for a pH of 7.20; this curve (pH = 7.2) was used for the computation. The permeability of oxygen in medical grade silicone rubber was obtained from reference 29. Buckles' experiment was conducted to measure only the oxygen transport. The partial pressure of carbon dioxide in the blood and the pH were maintained constant along the tube.

The diffusivity of oxygen in whole blood for H = 26 was computed using equation (29), $D_o = 1.38\ 10^{-5}$ cm^2/sec. Figure 7 is a plot of Buckles' experimental data and theoretical curve. The numerical agreement between Buckles' data and the theoretical prediction for $\beta = 0$, suggests that in this case the rotation-induced diffusion is insignificant when compared with the ordinary diffusion due to concentration gradients.

Table II. Buckles' Experimental Data with Human Whole Blood

L	=	39.5 cm	Hb. conc.	=	9.1 gm% (H=26)
OD	=	0.0636 cm	Temp.	=	38°C
ID	=	0.0305 cm	pH	=	7.14
Input pO_2	=	0-mm Hg	Input pCO_2	=	36-mm Hg
Outside pO_2	=	686-mm Hg	Outside pCO_2	=	36-mm Hg

No.	Q cc/min	pO_2 mm Hg	PS
1	0.521	13.8	16.0
2	0.521	11.8	12.5
3	0.1054	56.1	81.0
4	0.0521	544.0	100.0
5	0.521	18.7	25.8
6	0.210	32.1	51.9
7	0.1054	47.7	74.2

4.3 Comparison with Weissman and Mockros' Experimental Data and Theoretical Results

These investigators (ref 3) used freshly collected cattle blood in their experiments. Unfortunately, they did not measure the hemoglobin concentration in most of their experiments and the pH was not reported. The data plotted in figure 8 are for an initial saturation of 75 percent. The tube geometrical characteristics are L = 182.9 cm, ID = 0.08 in., OD = 0.09 in. The tube was made of silicone rubber (medical grade). Weissman and Mockros fitted their theoretical result to the data, using a diffusivity $D_o = 0.883 \times 10^{-5}$ cm^2/sec. Their result is shown in figure 8.

A pH of 7.4 was assumed for the effects of our computation. As before, the carbon dioxide partial pressure was in equilibrium with the gas outside the tube and no carbon dioxide transfer was allowed. Table III shows a comparison between cattle and human blood dissociation curves at pH = 7.4. Since both curves are quite close in the 75-to 100-percent range, the already known parameters of the human dissociation curve were used in our computation.

The ordinary diffusivity was computed using equation (29), assuming a hematocrit of 40 and a hemoglobin concentration of 14.5-g percent inside the red cells. These values are in the normal range of cattle blood. The computed value is $D_o = 1.15 \times 10^{-5}$ cm^2/sec. As before, the agreement between predicted value and laboratory data is excellent for $\beta=0$. The reader should be cautioned not to compare the D_o values and conclude that figure 8 shows it as an unimportant parameter. It must be reemphasized that the model of Weissman and Mockros assumes a boundary condition of no membrane resistance to the gas transport. Hence, their lower value of D_o, obtained by a curve fit, is merely implicitly including the added resistance due to the membrane.

Table III. Comparison between Cattle and Human Blood Oxygen Dissociation Curve at pH = 7.4 and T = 37°C.

	pO_2 mm Hg	
PS	Cattle	Human
75	43	40.9
80	47	45.7
85	52	51.7
90	60	61.4
95	75	81.4

4.4 Internal Profiles and Bulk Average Values of pH, Carbon Dioxide, and Oxygen in Oxygenation of Standard Venous Human Blood.

The application of the model introduced in this paper to the gas transport in standard venous human blood (ref 30) is illustrated in the example presented below. Since no indication of significant augmented diffusion has been found in the data obtained by Buckles (ref 2) or those obtained by Weissman and Mockros (ref 3), it was assumed that this phenomenon is insignificant in the normal oxygenation flow range. It was also assumed that the velocity profile is parabolic, which is a good approximation for $Q/R^3 > 192$ sec^{-1}. The tube characteristics, as well as the initial and boundary conditions are given in table IV.

The radially averaged or bulk average oxygen percent of saturation, carbon dioxide partial pressure, and pH versus the dimensionless length are shown in figure 9. The graph shows that 95-percent saturation, which is the normal arterial level, is reached at about $Z^* = 0.4$. On the other hand, the normal arterial level of the carbon dioxide partial pressure is about 40-mm Hg. This value is reached at $Z^* = 0.23$. These results indicate that in this case the limiting design phenomenon is the oxygen transport and not the carbon dioxide removal. The pH curve slowly increases from 7.4 to a value of 7.55 at $Z^* = 0.4$, which is the dimensionless length corresponding to arterial conditions.

Figure 10 shows the internal (unmeasured) profiles of carbon dioxide partial pressure and pH function of the dimensionless length, Z^*, and the dimensionless radius, r^*. The carbon dioxide family of curves shows that the carbon dioxide depletion occurs mainly in the outer layers of blood. The partial pressure of this gas at the center of the tube stays almost constant in the neighborhood of 50-mm Hg (initial value). The partial pressure at the wall ($r^* = 1$) is between 15- and 9-mm Hg for most of the tube length. This result indicates an overall carbon dioxide transport driving force of 50-mm Hg (0-mm Hg outside of the wall and 50-mm Hg at the center of the tube), the average wall loss is about 25 percent (12-mm Hg). The pH curves show that the value close to the wall may be considerably higher than the average bulk pH value. This enhances the oxygen bonding capability of the red cells by displacing the oxygen dissociation curve.

Figure 11 shows the internal oxygen profile as a function of r^* and Z^*. At $Z^* = 0.5$, which is the dimensionless length corresponding to about 100-percent saturation (fig. 9), the advancing oxygen front has not yet reached the center of the tube which is still at the initial condition, 30-mm Hg, but the blood in the outer layers is fully saturated ($pO_2 > 315$-mm Hg). The partial pressure of oxygen at the wall ($r^* = 1$) is about 700-mm Hg. This is a reduction of 8 percent in the overall oxygen transport driving force (730-mm Hg).

Table IV. Input Parameters for the Computerized Solution of the Oxygenation of Standard Venous (ref 30) Human Blood

Blood:	
Hematocrit	42
Hemoglobin conc.	15 g percent
D_o	1.11×10^{-5} cm^2/sec
pH	7.4
pO_2	31-mm Hg (60-percent saturation)
pCO_2	50-mm Hg
Oxygenator Atmosphere:	
pO_2 outside tube	760-mm Hg
pCO_2 outside tube	0
Tube:	
Material	Silicone Rubber (medical grade)
O_2 permeability (ref 29)	1210 $\frac{cc\ (STP)\ mil}{min\ m^2\ atm}$
CO_2 permeability (ref 29)	6310 $\frac{cc\ (STD)\ mil}{min\ m^2\ atm}$
R	0.01524 cm
OR	0.031 5 cm

It is concluded from this that the wall effect is more significant in the carbon dioxide than in the oxygen transport. However, in designing an oxygenator for the conditions described in table I, the oxygenation is of primary importance, since the carbon dioxide removal to standard arterial level is accomplished before the standard oxygen saturation arterial level is reached.

4.5 Parametric Analysis and Design Equation

A parametric analysis was conducted to determine the effect of hemoglobin concentration, hematocrit, pH, initial conditions, diffusivity, flow rate, and the tube characteristics (thickness, permeability, radius, and length) on the blood oxygen saturation. For this parametric analysis, the augmentation effect on diffusion due to the rotating erythrocytes was assumed insignificant. Also, the blood was considered a Newtonian fluid with a parabolic velocity profile. These are reasonable simplifications for the range within which most oxygenators of this type would be designed. The hemoglobin concentration Hm related to the hematocrit H by $Hm = 35.5/H$, where 35.5 is the concentration of hemoglobin inside the red cells in g percent (ref 31).

Theoretical results were obtained for a wide range of initial and boundary conditions. An analysis of these results showed that the increment in oxygen percent of saturation from the initial venous blood saturation ΔPS could be represented by an exponential function of the dimensionless length Z*. In order to use one function for any initial and boundary conditions within a limited range, the form of this function was chosen as $\Delta PS = A(B\ Z^*)^C$ where C is a constant, and A and B are parameters dependent on the other dimensionless parameters that affect the gas transport (wall characteristics, hematocrit, and initial oxygen saturation). The particular function chosen was the simplest form that represented the computer results with reasonable accuracy. This expression allows the design of steady-flow capillary tube oxygenators without the use of a computer.

The computer results were plotted on logarithmic paper, and it was found that the average value of the exponent C was 0.537. It was also found that the value of the parameter B was independent of the hematocrit and wall characteristics and could be simply described by $B = 1 - PS_v/100$. Figure 12a shows the increment in oxygen percent of saturation predicted by the computer for several initial values of venous oxygen percent saturation and for certain given hematocrit and wall characteristics shown in the figure where the tube material is silicone rubber (medical grade). In the figure, ΔPS is plotted against $(B\ Z^*)$. Figure 12a shows that the majority of the points predicted by the computer are in a single straight line with a slope of 0.537. The points farthest from the average straight line are those corresponding to the lower initial venous blood saturations (0 and 30 percent).

These points have the least practical value, since most oxygenators are designed for initial saturations above 45 percent. In any case, these points are only 2 or 3 units of saturation from the straight line representing the majority of the computer results. Figure 12a also shows that the pH effect on ΔPS for pH between 7.3 and 7.5 is insignificant. Figures 12b through 12e are similar to figure 12a but for different hematocrits and/or tube characteristics.

After plotting the intercept of these lines at B $Z^* = 1$ versus the hematocrit and tube characteristics as given in the third boundary condition for equation (30) for $F_4 = 1$ (no interfacial resistance), it was found that A could be approximately described by $A = [155.4 - 1.3\ H - 1.5 \ln OR^*/P_m\ 10^{-4}]$. Substituting the values of A, B, and C into the empirical equation describing the change in oxygen percent of saturation yields

$$\Delta PS = [155.4 - 1.3\ H - 1.5 \ln OR^*/P_m 10^{-4}]\ \Delta PS^* \qquad (48)$$

$$\Delta PS^* = [(1 - PS_v/100)\ Z^*]^{0.537} . \qquad (49)$$

The factor 1.5 includes an average oxygen diffusivity and the oxygen solubility in blood so that the last term is dimensionless. In equation (48) the permeability of the wall P_m must be used in cc (STP) mil/m^2 atm min.

Figure 13 is a plot of equation (49). The data obtained by the author using rejuvenated 21-day-old human blood and the data obtained by other investigators (ref 2,3) are also shown in the figure. The experimental venous and arterial data obtained by the author and the arterial values predicted by the model are given in table V.

Figure 13 implies that the transport characteristics of rejuvenated 21-day-old blood are close to the transport characteristics of fresh blood, although some other physiological properties may be changed.

5. SUMMARY AND CONCLUSIONS

A mathematical model for the transport of oxygen and carbon dioxide in semipermeable tubes under steady-flow conditions has been developed. The model considers the blood as a non-Newtonian fluid, and assumes the sink reaction rate with the gases to be negligible compared with the gas diffusion time through the plasma. The model considers the membrane resistance to the gas transport, including the possibility of an additional mass transport resistance due to interfacial phenomena (protein deposition, etc). The possibility of gas transport augmentation due to the rotation of the erythrocytes

TABLE V

Steady-Flow

Experimental Data and Predicted Arterial Values

L = 24.8 cm H = 29

OD = 0.0940 cm Temp = 37°C

ID = 0.0508 cm No. Tubes = 31

Membrane: Medical grade silicone rubber

No.	Q cc/min	Venous				Arterial				Predicted arterial		
		pH	pCO_2	pO_2	PS	pH	pCO_2	pO_2	PS	pH	pCO_2	PS
1	6.5	7.34	46	27	48	7.36	41	45	77	7.41	39	75
2	9.6	7.39	45	27	50	7.41	43	38	72	7.43	39	71
3	12.4	7.37	50	29	54	7.38	40	40	72	7.41	46	71
4	18.5	7.36	51	27	48	7.38	46	36	67	7.40	47	64

* Partial pressures in mm Hg.

in the velocity field is also included. The ordinary diffusivity of the gases in whole blood was determined by using an equation developed by Fricke (ref 27), together with the data obtained by several other investigators (ref 13,24). The numerical solution of the transport partial differential equation was obtained by approximating these equations by finite difference equations and using a digital computer. The oxygen and the carbon dioxide differential equations were simultaneously solved and the pH computed for any point in the tube. The model's prediction showed excellent agreement with the data obtained by other investigators (ref 2,3) and that obtained by this author. Although explicitly included in the model, in processing the solution, the interfacial resistance and augmentive diffusion effects were considered negligibly small. The agreement between model predictions and experimental data was used in justifying this assumption. A simple design equation and generalized chart were developed using the computer results and curve-fitting techniques. The oxygen saturation computed from this equation agrees with the computer solution within two percent. Experimental data obtained using fresh blood and experimental data obtained using rejuvenated 21-day-old blood are plotted in the chart (fig. 13). The agreement among these groups of data suggests that the gas transport characteristics of rejuvenated 21-day-old blood is the same as that of fresh blood, although other physiologic characteristics may be changed.

The numerical solution of the steady-flow differential equation was obtained for standard venous blood initial conditions (ref 30). Charts showing the predicted pH, carbon dioxide, and oxygen profiles as functions of the dimensionless length and radius, and their bulk average values are included.

The steady-flow dimensionless differential equation shows that if the velocity profile is assumed parabolic ($Q/R^3 > 200\ sec^{-1}$), and if the rotation-induced diffusivity is assumed insignificant, the arterial saturation is independent of the tube diameter. In practice, the entrance effect on the velocity profile should be considered.

The design equation shows that for silicone rubber tubes a change in the ratio of the outside diameter to the inside diameter (OR*) of 2 to 1 produces a change of less than 5 percent in the oxygen saturation.

The model predicts that the carbon dioxide removal to standard arterial level (ref 30) is accomplished before the standard oxygen saturation arterial level is reached. This result suggests that the blood oxygenation is the limiting phenomenon in designing tubular oxygenators.

6. LITERATURE CITED

(1) Galletti, P. M. and G. A. Brecher, Heart-Lung Bypass, Grune & Stratton, New York 1962.

(2) Buckles, R. G., Ph.D. Thesis, MIT, Cambridge, Mass. 1966.

(3) Weissman, M. H. and L. F. Mockros, J. of Eng. Mech., Div. Proc. ASCE, 225 1967.

(4) Marx, T. I., E. S. Warren, D. SJ. Andrews, and E. M. Calvin, J. Appl. Physiology, Vol 15, 1123, 1960.

(5) Bradley, C. G., and R. W. Pike, Proc. 21st ACEMB 1968.

(6) Buckles, R. G., E. W. Merrill, and E. R. Gilliland, AIChE J. 703, Vol 14, No. 5, 1968.

(7) Thews, G., Pflügers Archiv. 265, 138, 1967.

(8) Casson, N., Rheology of Disperse Systems, Mill, C. C. (Editor), Pergamon Press, Oxford, 1959.

(9) Schollander, P. F., Science, 131, 585 (1960).

(10) Roughton, F. J. W., Oxygen in the Animal Organism, Dickens, F. and E. Neil (Editors) p 5-27, IUB. Symp. Series, 31 (1963c).

(11) Perutz, M., Nature (Lond), 161, 204, 1948.

(12) Prankerd, T. A. M., The Red Cell, Thomas, Springfield, Ill. 1960.

(13) Klug, A., F. Freuzer, F. J. W. Roughton, Helvet Physiol et Pharmacol, Acta, 14, 121. 1956.

(14) Keller, K. H., E. F. Leonard, 12th Advanced Seminar AIChE, Part I, 152, 1968.

(15) Keller, K. H., S. K. Friedlander, J. of General Physiology, Vol 49, 4, 663-679, 1966.

(16) Spaeth, E. E., and S. K. Friedlander, Biophysical J., Vol 7, No. 6, 827-851, 1967.

(17) Lightfoot, E. N., AIChE J., Vol 14, 4, 669, 1968.

(18) Jones, A. L., Biorheology, Vol 3, 183-188, 1966.

(19) Merrill, E. W., A. M. Benis, E. R. Gilliland, T. K. Sherwood, and E. W. Salzman, J. Appl. Physiol, 20 (5), 954-967, 1965.

(20) Dorson, W. J. and D. Hershey, Blood Flow Through Long Capillary Tubes, 62nd National Meeting, AIChE (1967).

(21) Handbook of Respiratory Data in Aviation, Material Research Council, Committee on Aviation Medicine Subcommittee on Oxygen, Office of Scientific Research and Development, Washington, 1944.

(22) Physiology Study Notes, Staff of the Physiology Department, Northwestern University Medical School, 1964 edition (see ref 3).

(23) Goldsmith, H. L., S. G. Mason, Rheology Vol IV, Acad. Press, N.Y. (1967).

(24) Hershey, D., T. Karhan, AIChE J., 969, Vol 14, No. 6 (1968).

(25) Thews, G., Pflüger Arch-ges, Phisiol, 268, 308 (1959).

(26) Kreuzer, F., and W. Z. Yahr, J. Appl. Physiol., 15, 1117 (1960).

(27) Fricke, H., Physical Rev., 24, 575, 1924.

(28) Perry, R. H., Chemical Engineers Handbook, 4th edition, McGraw-Hill, New York (1963).

(29) Galletti, P. M., M. T. Snider, and D. Gilber-Aiden, Medical Research Eng., 20, Vol 5, No. 2 (1966).

(30) Lanham, C. E., F. Villarroel, and J. M. Calkins, presented at 1st International Symp. on Blood Oxygenation, Cincinnati (1969).

(31) Blood and Other Body Fluids, ASD Technical Report, 61-199, Washington, D. C., 1961.

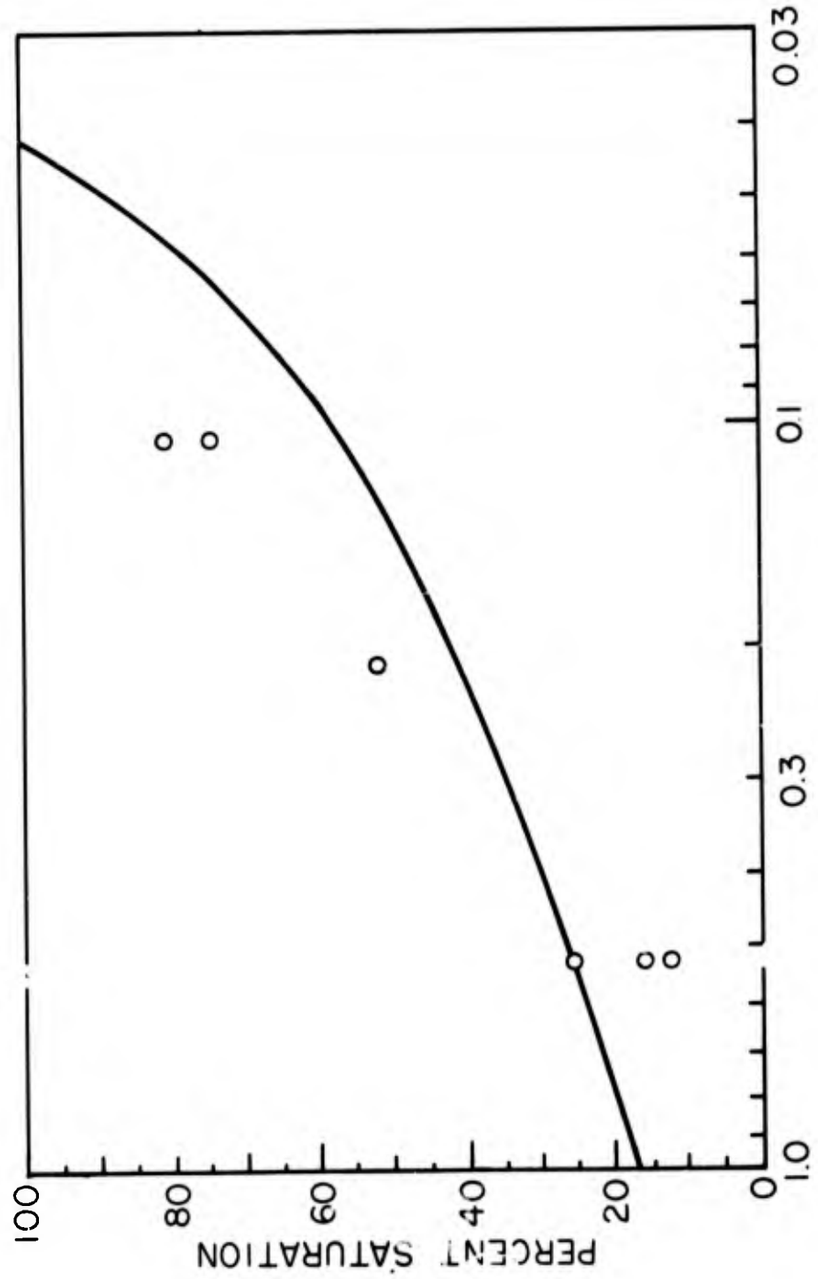

Figure 1. Data obtained by Buckles (ref 2) and curve predicted by Buckles' model.

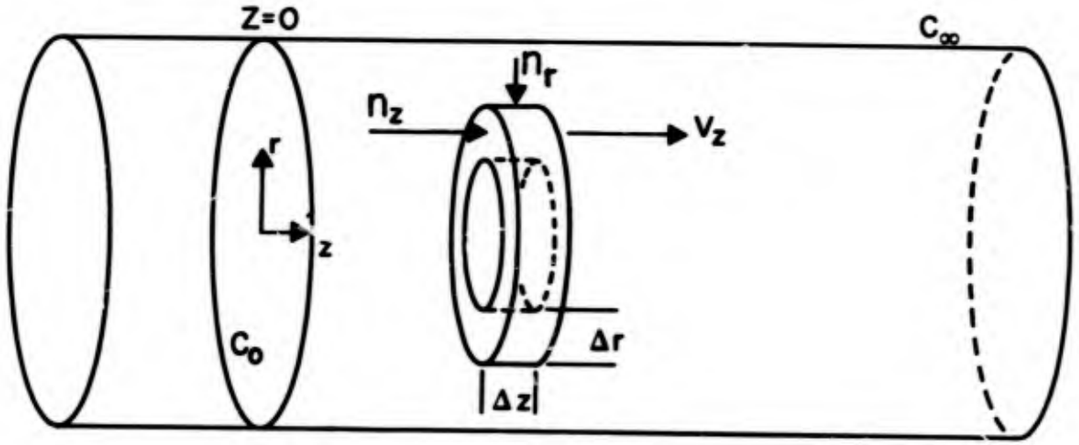

Figure 2. Annular ring over which mass balance is made to get differential equation for the concentration distribution in the gas exchanger.

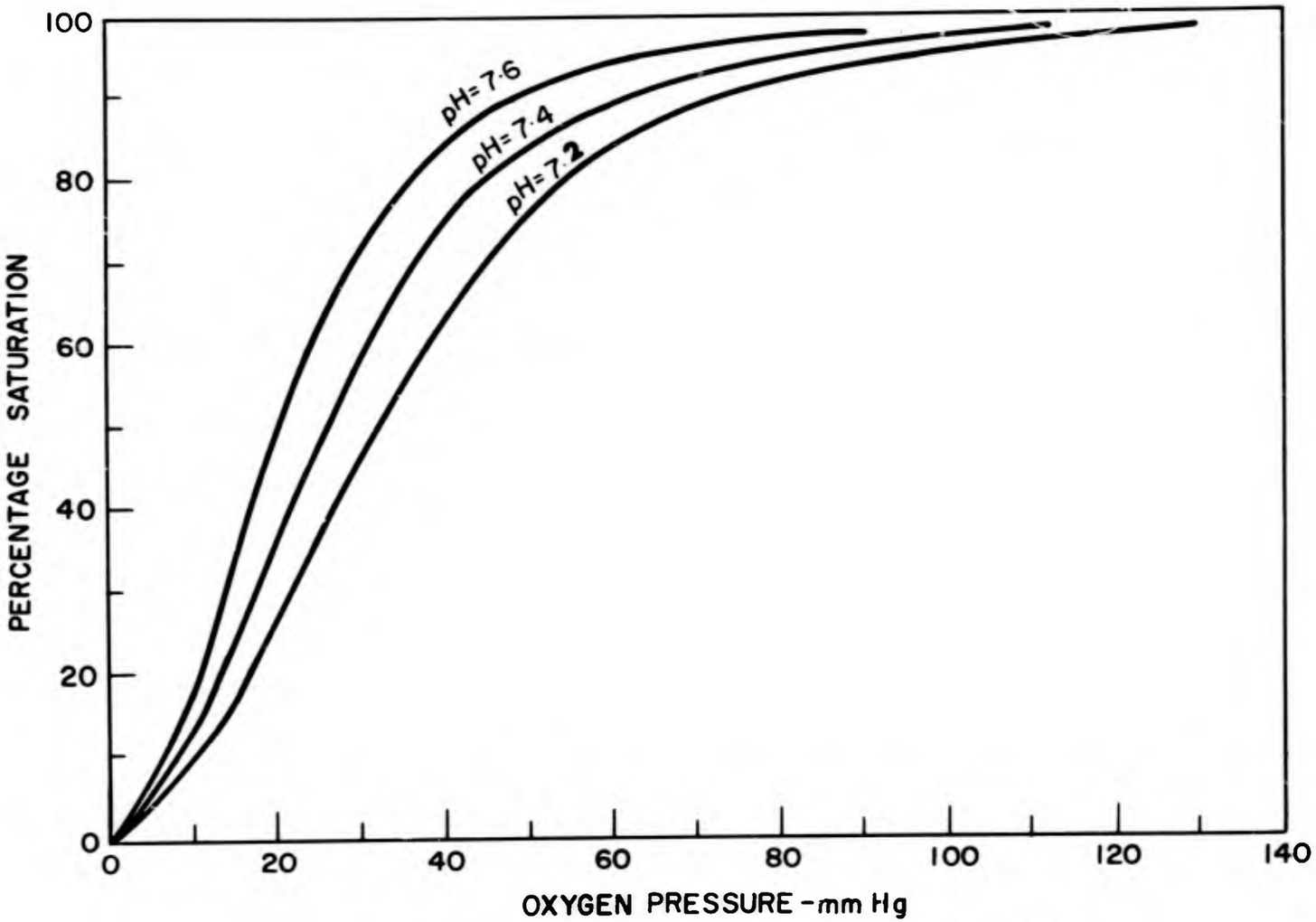

Figure 3. Oxygen dissociation curve for human blood (ref 21).

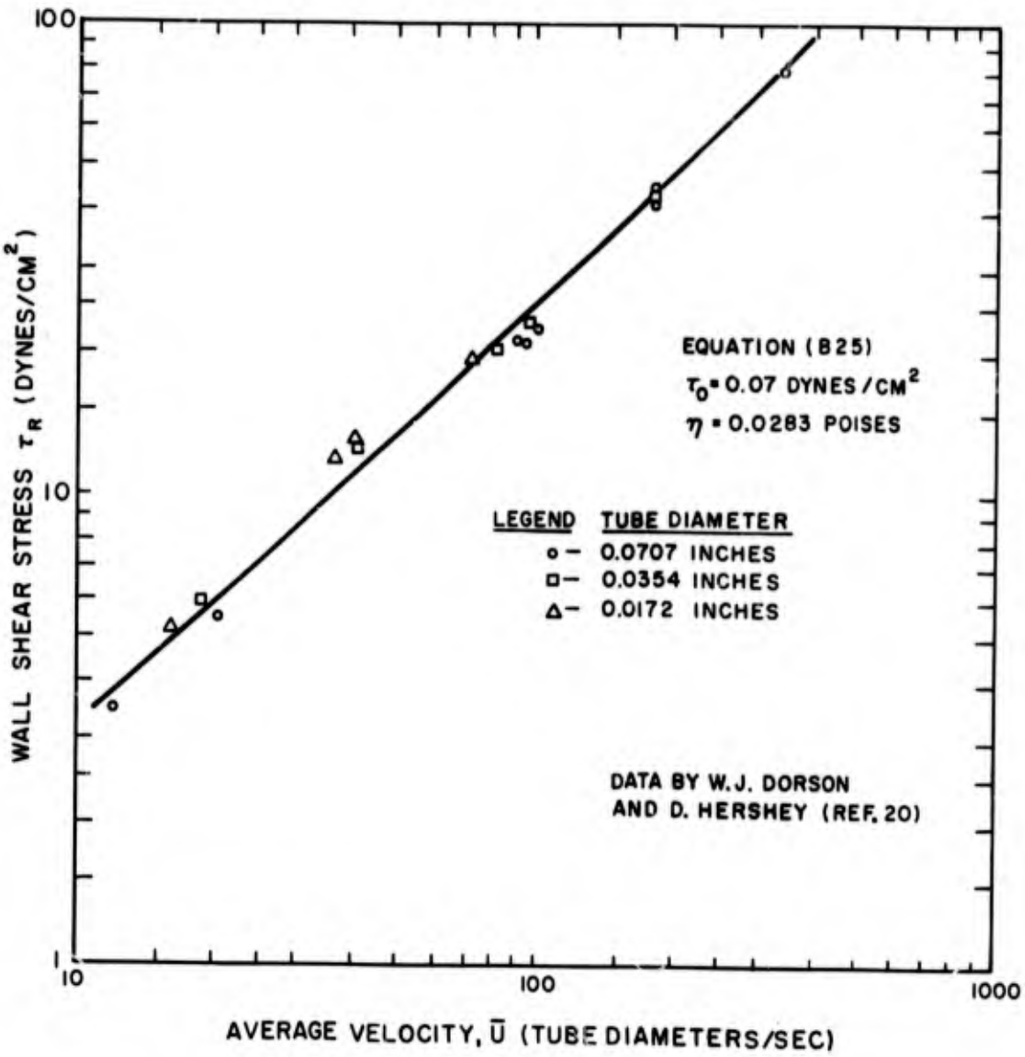

Figure 4. Data obtained by Dorson and Hershey (ref 20) and equation (B-24).

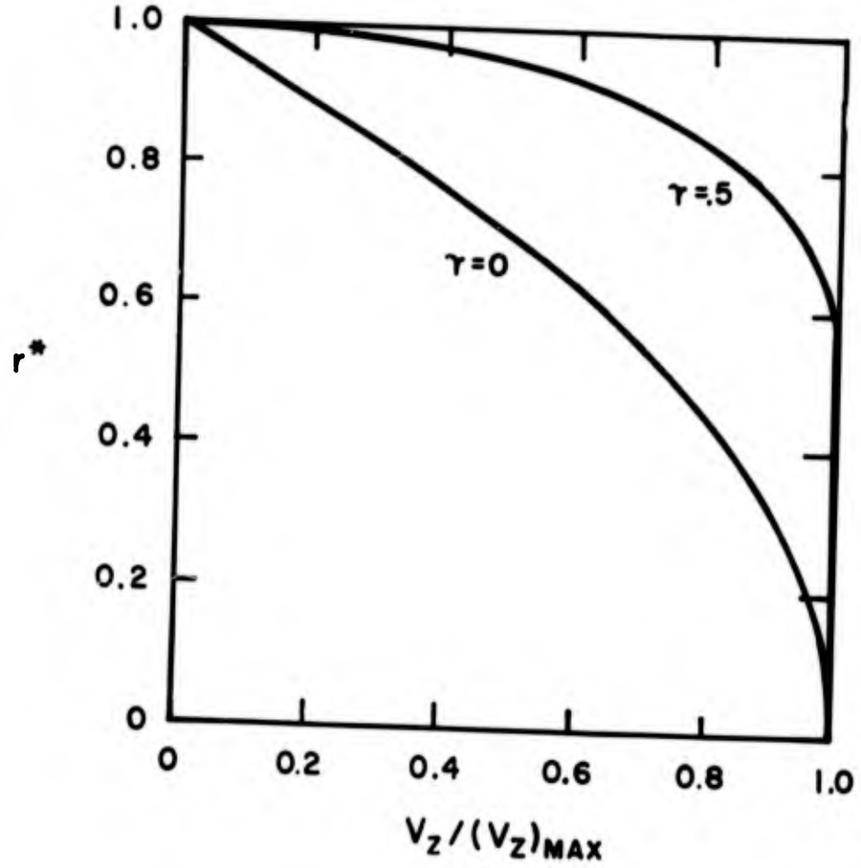

Figure 5. Dimensionless velocity for $\gamma = 0$ and $\gamma = 0.5$.

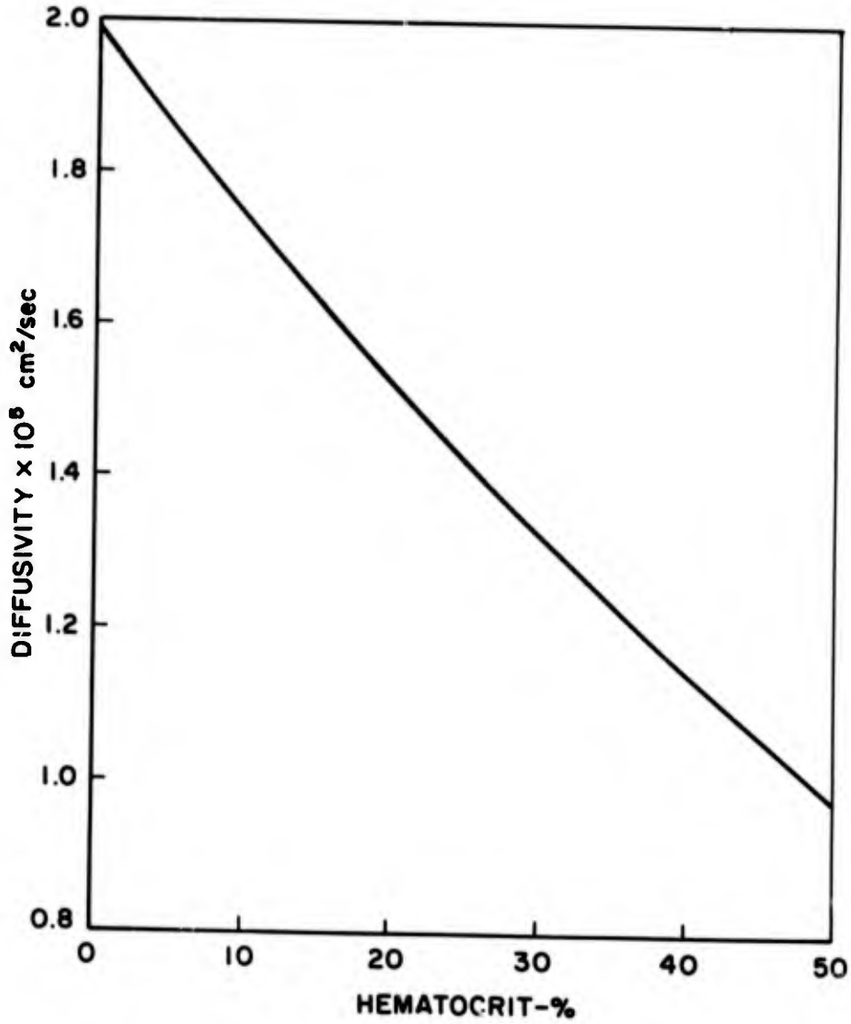

Figure 6. Diffusivity of oxygen in blood.

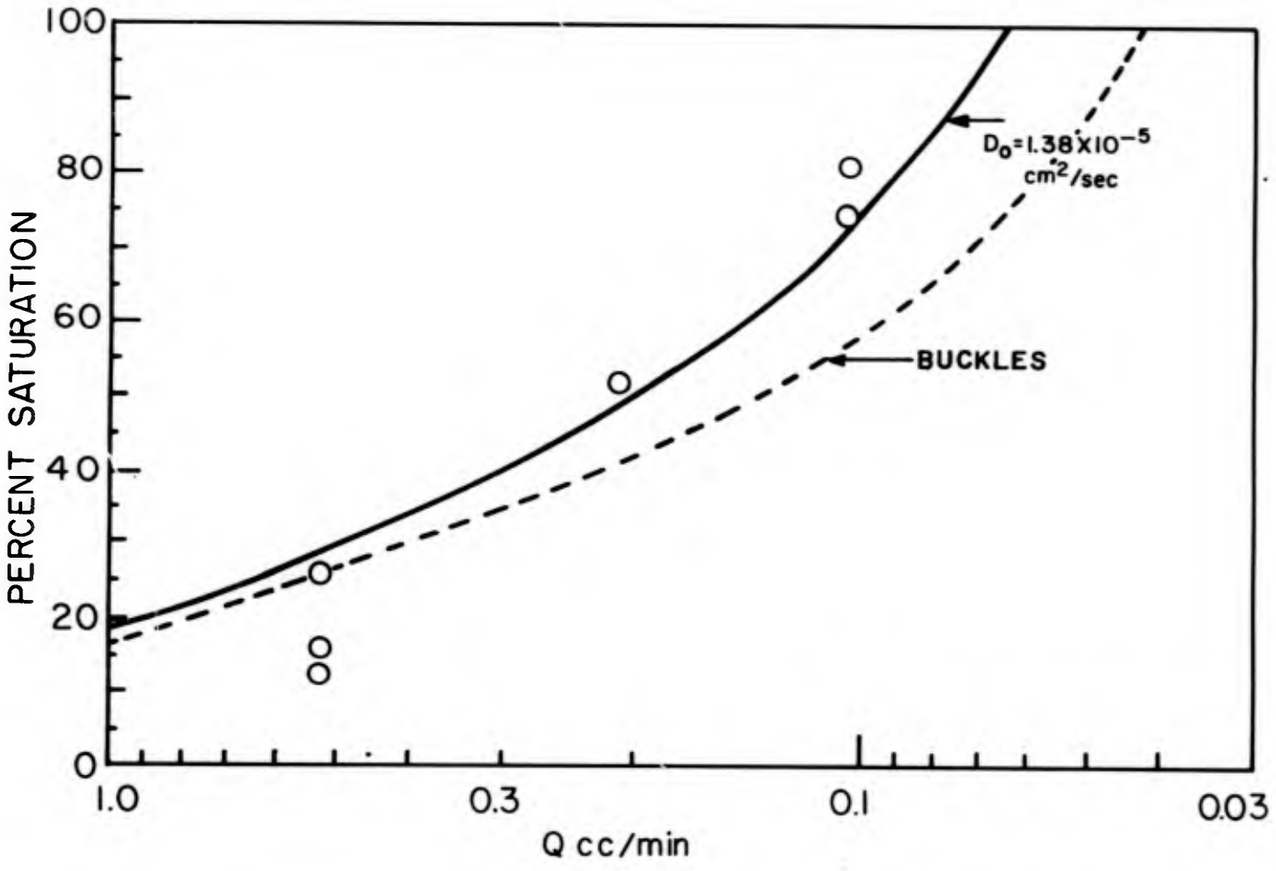

Figure 7. Comparison between the numerical solution of equation (30) and the data obtained by Buckles (ref 2).

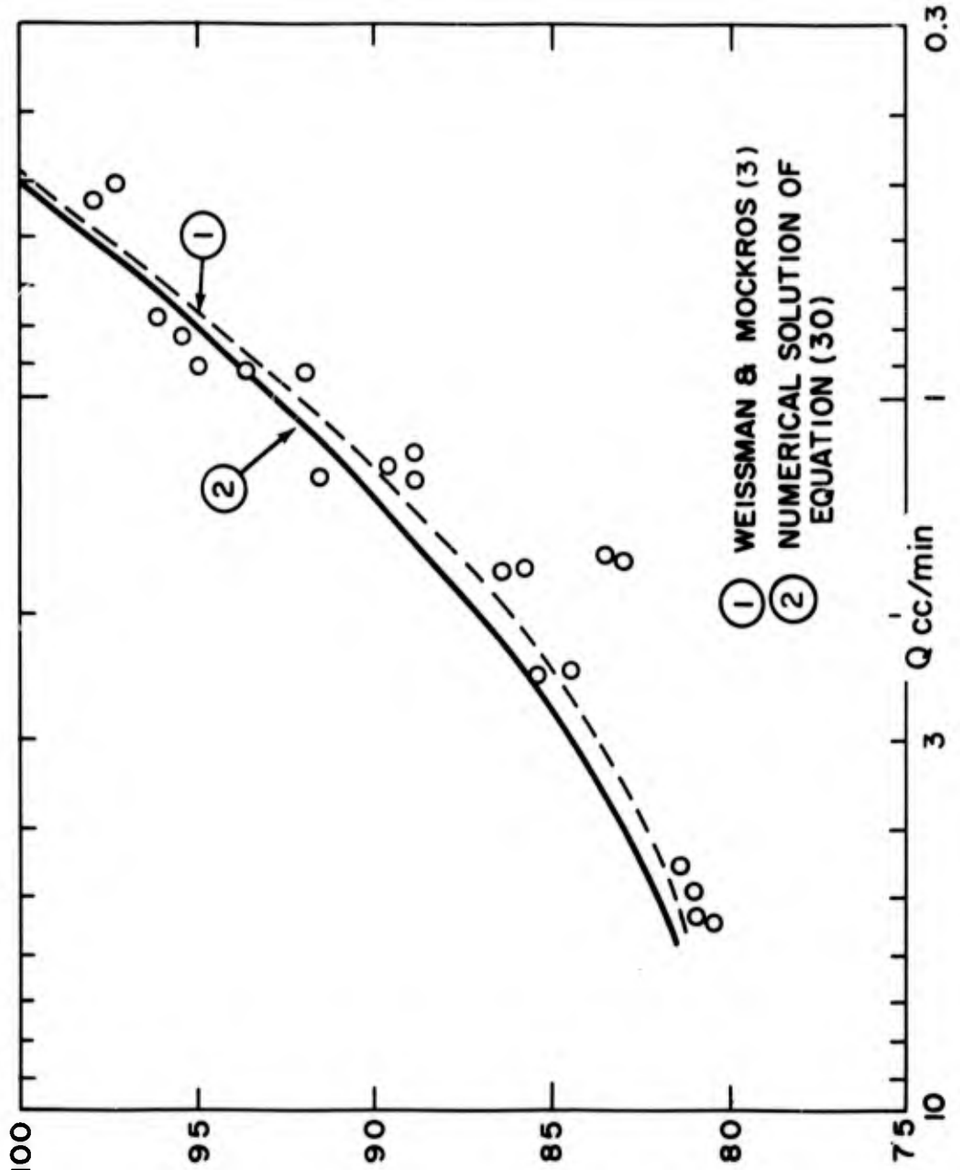

Figure 8. Comparison between the numerical solution of equation (30) and the data obtained by Weissman and Mockros (ref 3).

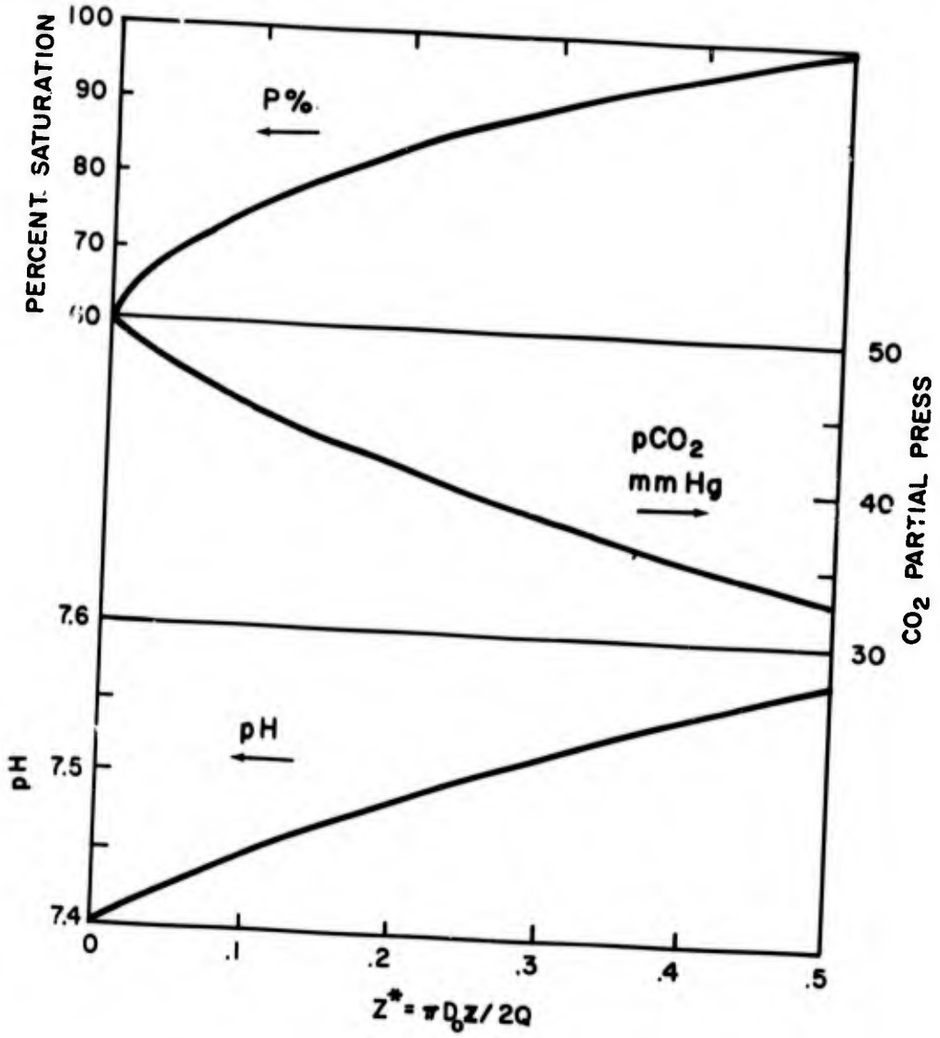

Figure 9. Radially averaged or bulk average oxygen percent of saturation, carbon dioxide partial pressure, and pH versus the dimensionless length in the numerical solution of the transport differential equation using standard venous blood conditions.

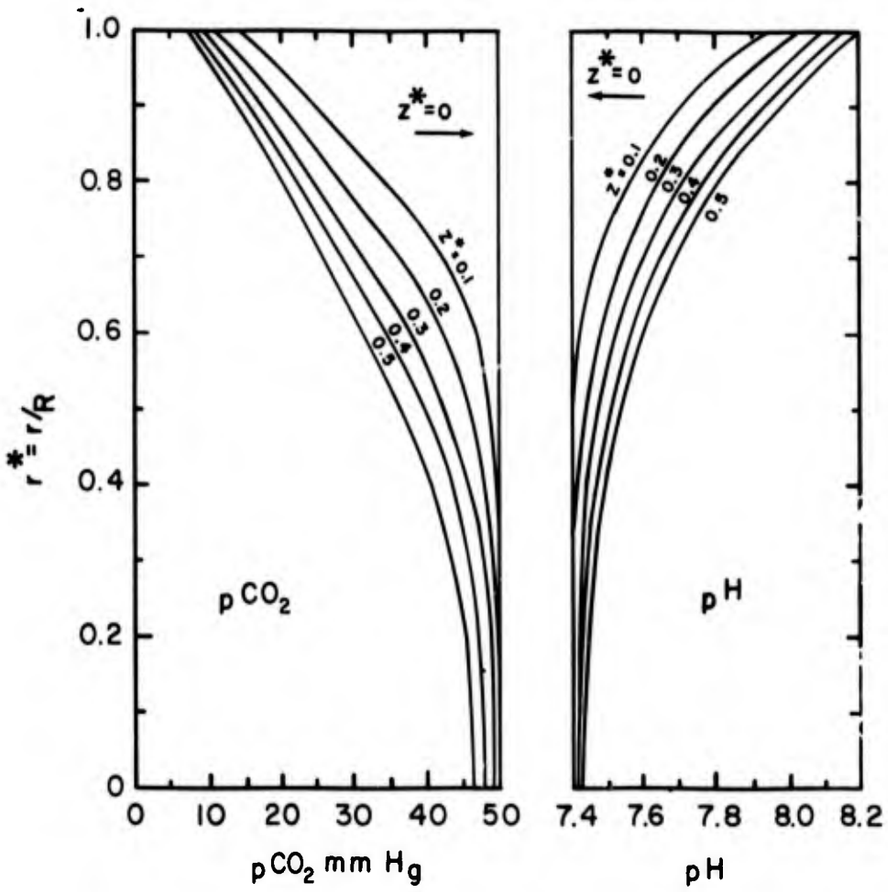

Figure 10. Internal (nonmeasurable) profiles of carbon dioxide partial pressure and pH function of the dimensionless length and the dimensionless radius.

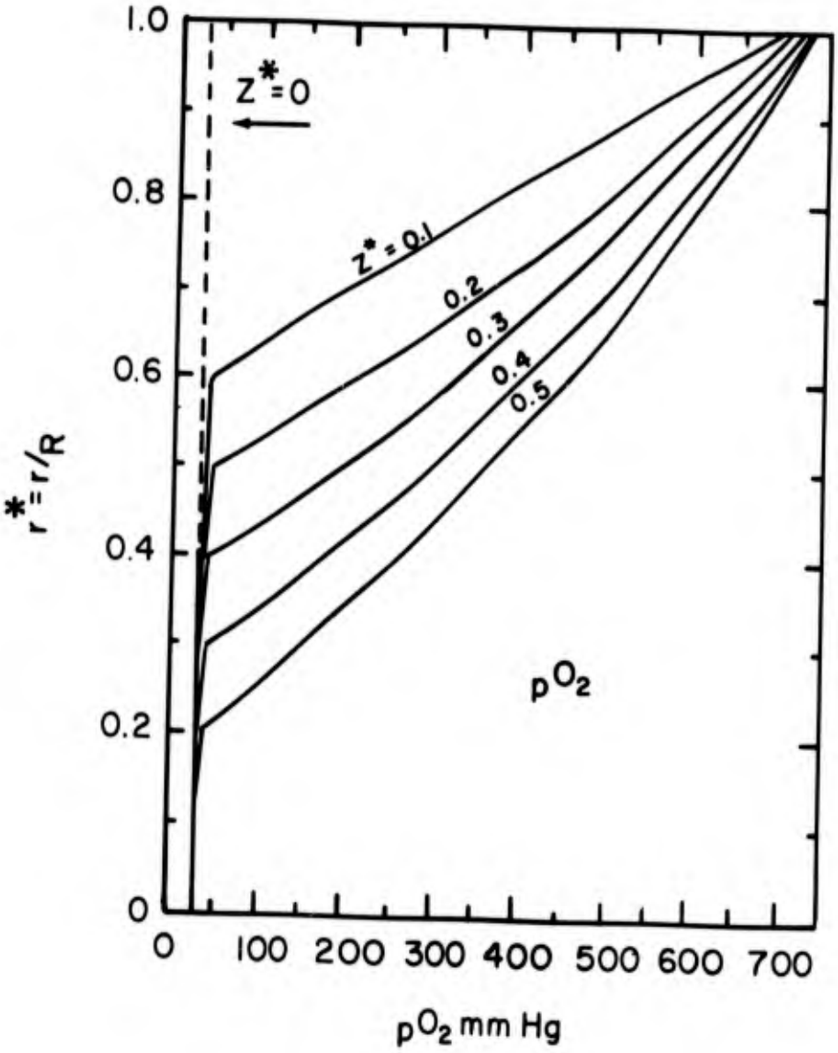

Figure 11. Internal oxygen profile function of the dimensionless length and the dimensionless radius.

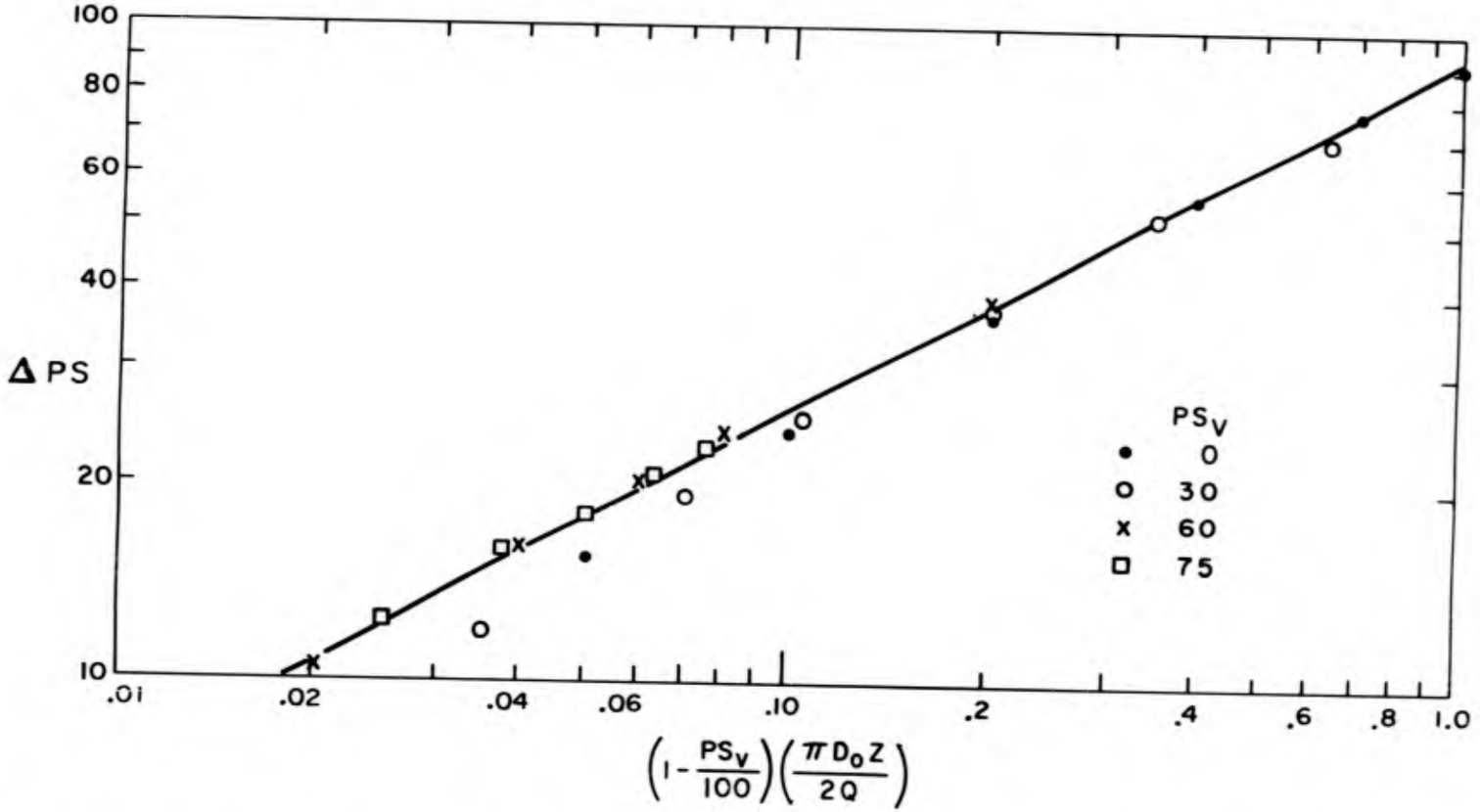

Figure 12a. Equation (49) and computer solution for Hm = 15-g percent, H = 42, pH = 7.3, 7.4, and 7.5 and OR* = 2.08. (The points shown are those predicted by the model.)

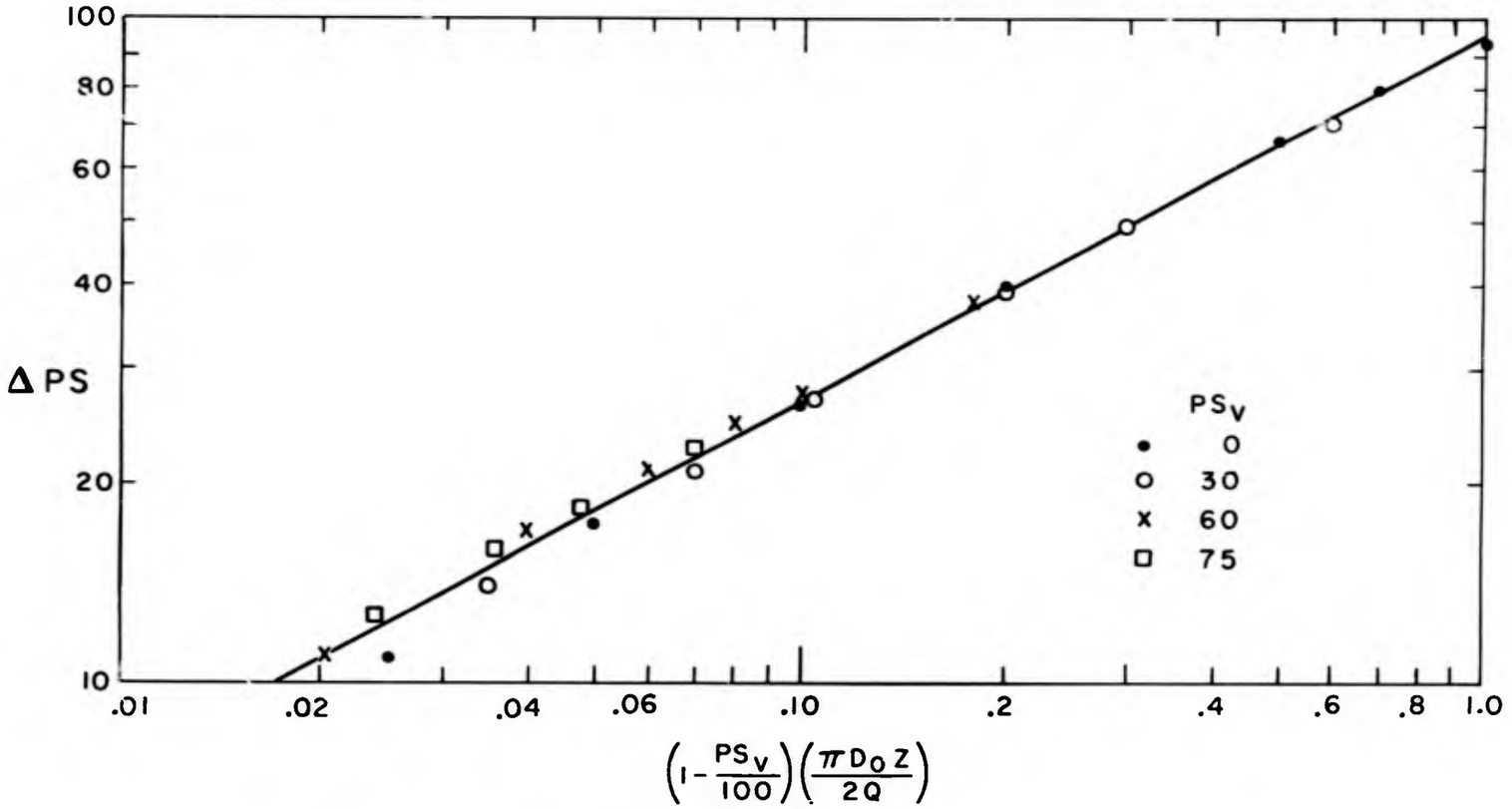

Figure 12b. Equation (49) and computer solution for Hm = 15-g percent, H = 42, pH = 7.4, and OR* = 1.328. (The points shown are those predicted by the model.)

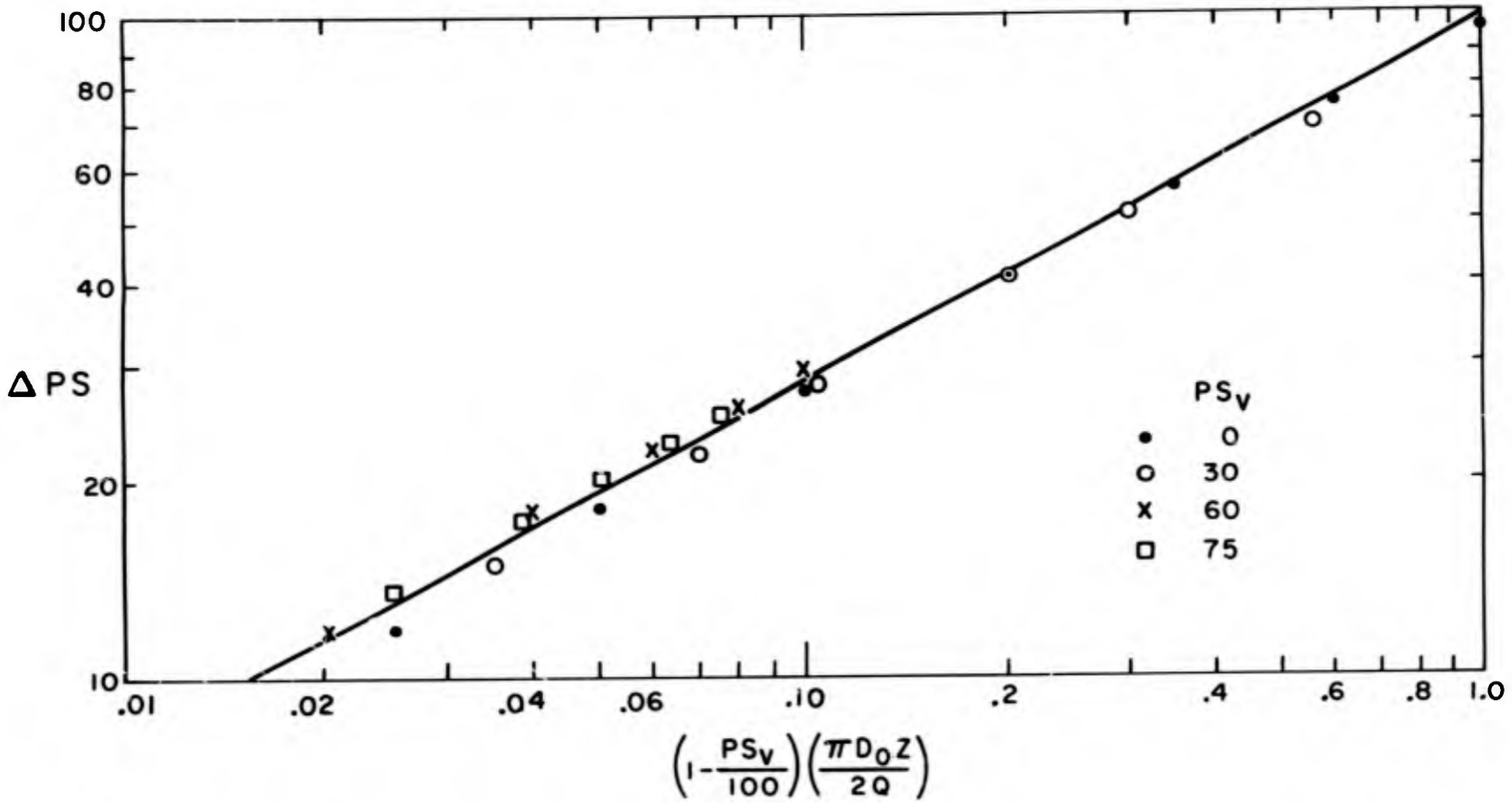

Figure 12c. Equation (49) and computer solution for Hm = 15 g-percent, H = 42, pH = 7.4, and OR* = 1.0. (The points shown are those predicted by the model.)

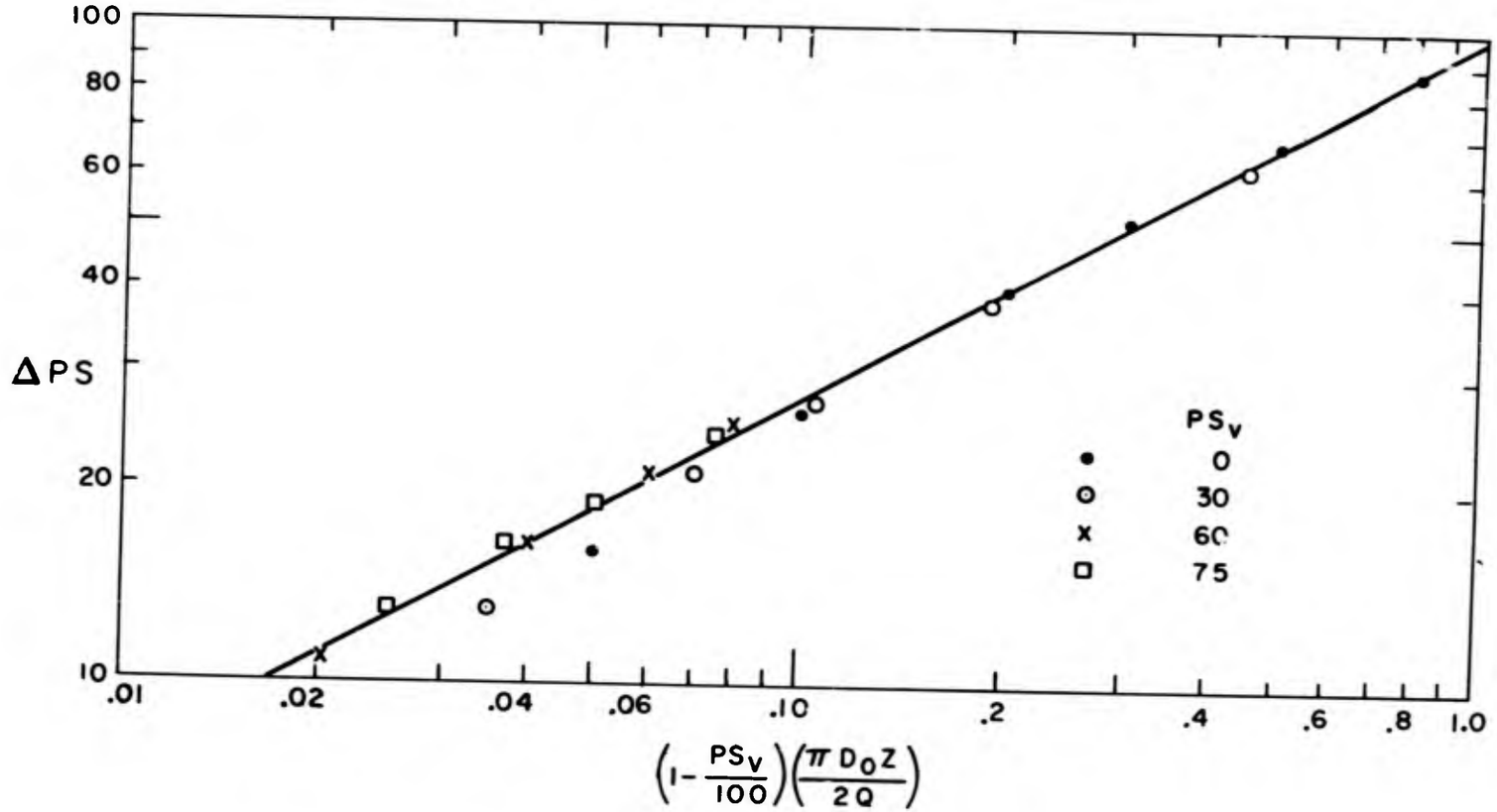

Figure 12d. Equation (49) and computer solution for Hm = 13.2-g percent, H = 37, pH = 7.4, and OR* = 2.08. (The points shown are those predicted by the model.)

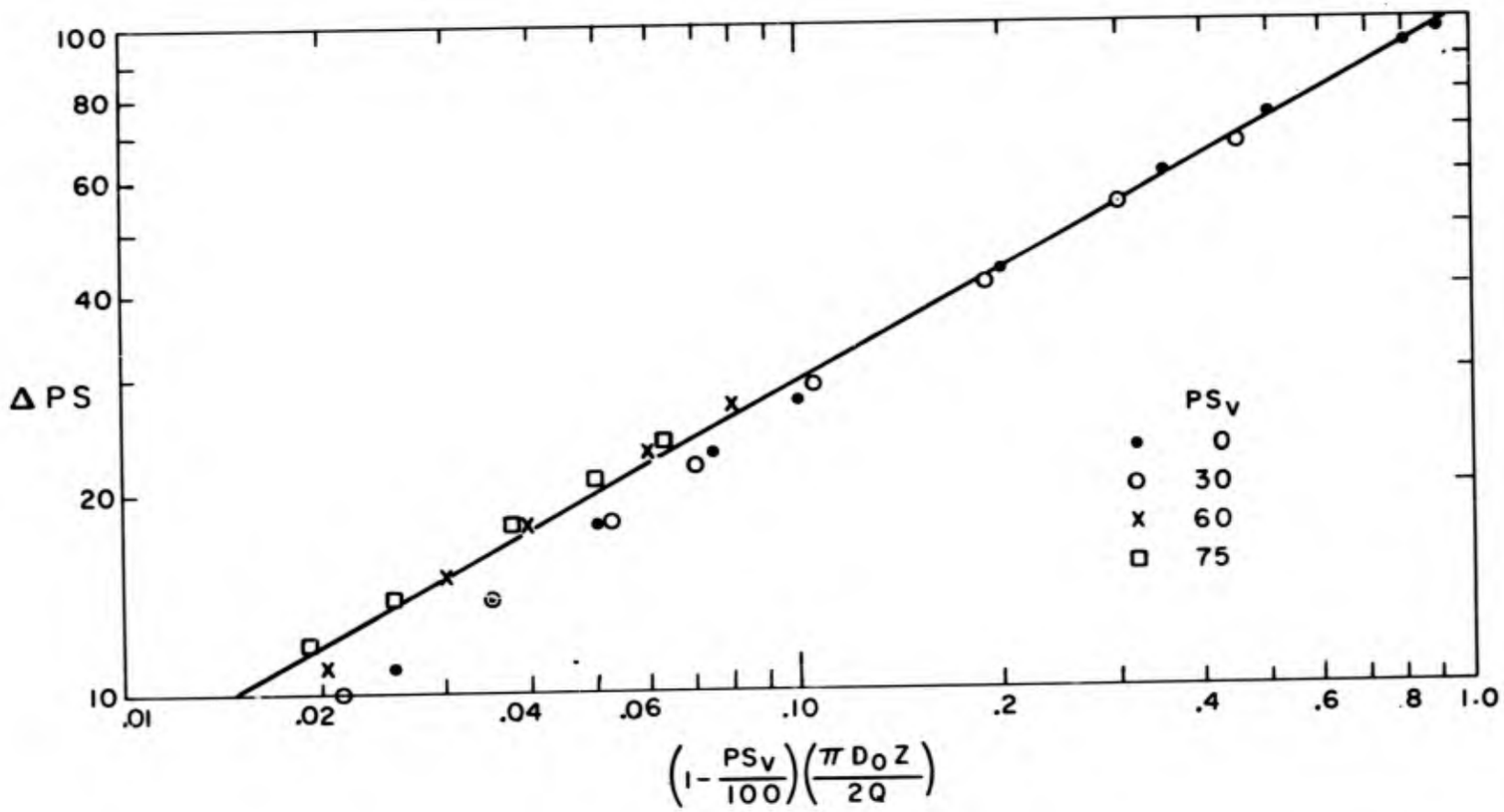

Figure 12e. Equation (49) and computer solution for Hm = 11.4-g percent, pH = 7.4, and OR* = 2.08. (The points shown are those predicted by the model.)

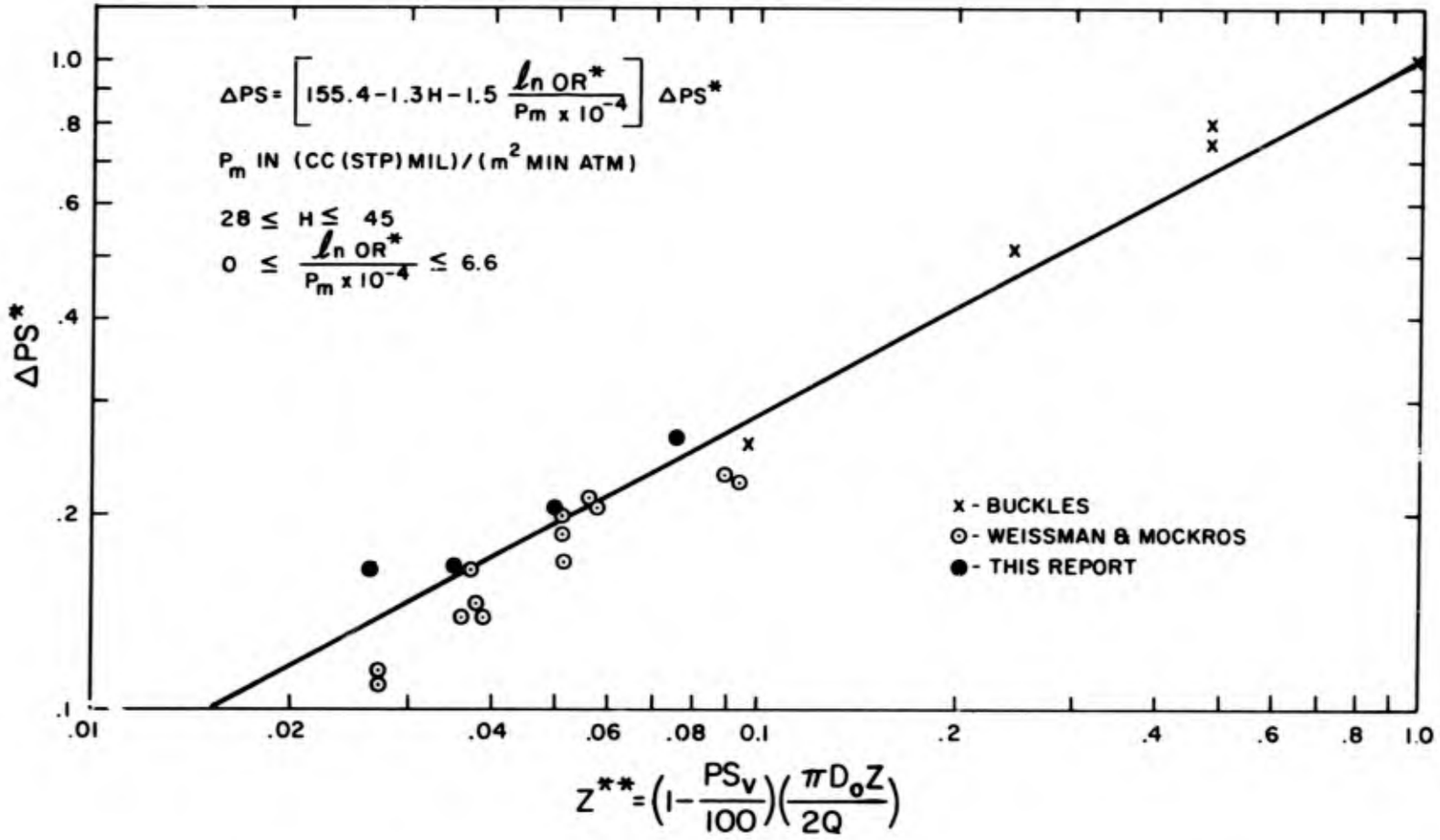

Figure 13. Design equation and generalized chart for oxygenation of blood under steady-flow conditions.

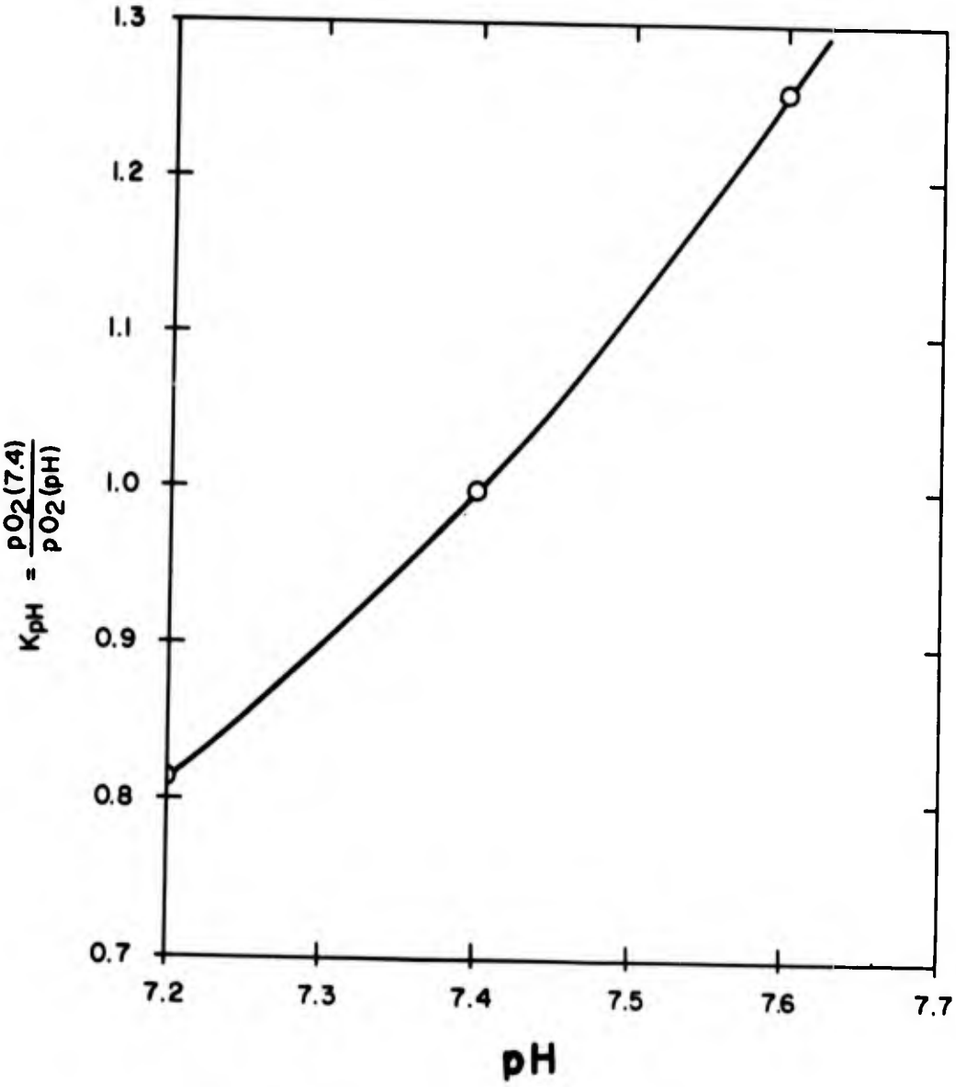

Figure 14. pH mapping factor.

APPENDIX A

OXYGEN DISSOCIATION CURVE

The equilibrium of the oxygen-hemoglobin reaction is described, empirically, by the blood oxygen dissociation curve. This curve is a plot of the percentage of oxygen saturation of the blood as a function of the plasma oxygen partial pressure. One hundred percent saturation is defined as the saturation at which the red cells reach their maximum oxygen content. Figure 3 (body of report) shows the standard blood oxygen saturation curve for three values pH. Table A-I shows the oxygen percent of saturation versus the oxygen partial pressure for three different pH. The figure also shows the ratio, K_{pH}, between the partial pressure at pH = 7.4 and the partial pressure at pH = 7.2 and 7.6 for all percent of saturation, PS,

$$K_{pH} = \frac{pO_2(PS, 7.4)}{pO_2(PS, pH)} \quad . \qquad \text{(A-1)}$$

Table A-I shows that the ratio between the oxygen partial pressures is quite independent of the oxygen percent of saturation. For example, $K_{7.2}$ is 0.814 and $K_{7.6}$ is 1.259 for all percent of saturation; the departure of the individual values of this ratio with respect to the average is well within the experimental error of the partial pressure given in the table. Figure 14 (body of report) is a plot of the partial pressure ratios K_{pH} versus the pH. The figure also shows a simple polynomial fit to the points. The relation representing the polynomial fit is

$$K_{pH} = 41.367 - 12.0225\ (pH) + 0.8875\ (pH)^2 \ , \qquad \text{(A-2)}$$

where K_{pH} superimposes the oxygen dissociation curve at any pH within the experimental range to that at pH = 7.4. In other words, the oxygen percent of saturation PS becomes a function f of the product (K_{pH} p O_2), and the function is given by the oxygen dissociation curve at pH = 7.4

$$PS = f(K_{pH}\ pO_2) \ . \qquad \text{(A-3)}$$

The oxygen partial pressure in mm Hg and the plasma oxygen concentration are related by[1]

$$pO_2 = 7.0\ 10^5\ C \ . \qquad \text{(A-4)}$$

From equations (A-3) and (A-4) ,

$$PS = f\left[\frac{W}{7.0\ 10^5}\right] \qquad \text{(A-5)}$$

---

[1]Roughton, F. J. W., Oxygen in the Animal Organism, Dickens, F. and E. Neil editors, pp. 5-27, IUB Symp. Series, 31 (1963c).

where

$$w = K_{pH}\, C \tag{A-6}$$

and C is in g-mole/liter.

The oxygen dissociation curve at pH = 7.4, f, was curve fitted in three parts:

(1) $w > 4.282\ 10^{-5}$ g-mole/liter, or $pO_2 > 30$-mm Hg at pH = 7.4

$$PS = 99.48 \exp\left\{\frac{5.473}{w}\ 10^{-6} - \frac{1.2878}{w^2}\ 10^{-9} + \frac{2.3709}{w^3}\ 10^{-15}\right\} \tag{A-7}$$

(2) $2.141\ 10^{-5} < w < 4.282\ 10^{-5}$, or $15 < pO_2 < 30$-mm Hg at pH = 7.4

$$PS = 1.628\ 10^{6}\ w - 11.2 \tag{A-8}$$

(3) $0 < w < 2.141\ 10^{-5}$ g-mole/liter, or $0 < pO_2 < 15$-mm Hg

$$PS = 5.95\ 10^{5}\ w + 2.352\ 10^{8}\ w^2 \quad . \tag{A-9}$$

Table A-1

Table of Percent of Saturation versus Oxygen Partial Pressure at pH 7.2, 7.4, and 7.6

Percent Saturation	pO_2 mm Hg					
	pH = 7.2	pH = 7.4	pH = 7.6	$K_{7.2}$	$K_{7.4}$	$K_{7.6}$
4	4.6	3.8	3.0	0.826	1.000	1.267
15	13.5	10.9	8.7	0.807	1.000	1.252
30	22.1	17.9	14.2	0.810	1.000	1.261
50	32.3	26.3	20.9	0.814	1.000	1.258
70	44.3	36.1	28.7	0.815	1.000	1.258
80	56.2	45.7	36.3	0.813	1.000	1.259
85	63.6	51.7	41.1	0.813	1.000	1.258
90	77.2	61.4	48.7	0.795	1.000	1.261
94	92.1	75.0	59.5	0.814	1.000	1.261
98	139.0	113.0	89.8	0.813	1.000	1.259
				Av: 0.814	Av: 1.000	Av: 1.259

APPENDIX B

VELOCITY PROFILE

In order to solve for the velocity profile of blood—a non-Newtonian fluid, flowing in a circular tube of constant cross-sectional area—the solution must satisfy the equation of motion plus any constitutive relations and boundary conditions. As previously stated, the following assumptions will be used.

Steady-flow conditions:

$$\frac{\partial V_z}{\partial t} = 0. \tag{B-1}$$

Laminar flow:

$$V_r = 0$$

$$V_\theta = 0 \quad . \tag{B-2}$$

The fluid is incompressible:

$$\frac{\partial V_2}{\partial Z} = 0 \tag{B-3}$$

The equation of motion in cylindrical coordinates for the r- and z-directions are

$$0 = - \frac{\partial p}{\partial r}$$

$$0 = - \frac{\partial p}{\partial Z} + \frac{1}{r} \frac{\partial}{\partial r}(r\tau), \tag{B-4}$$

where

$$\tau = \tau_{rz} \quad .$$

From equation (B-4), we see that the pressure is a function of the axial coordinate Z only. Reorganizing and integrating with respect to Z, we obtain

$$\frac{1}{r} \frac{\partial}{\partial r}(r\tau) = - \frac{\Delta p}{L} \ , \tag{B-5}$$

and integrating with respect to r,

$$\tau = - \frac{\Delta p}{L} \frac{r}{2} \tag{B-6}$$

rearranging equation (B-6),

$$\frac{-2}{\Delta p/L} = \frac{R}{\tau_R} \quad . \tag{B-7}$$

Then, from equations (B-6) and (B-7)

$$r = \frac{R}{\tau_R}\,\tau \quad , \tag{B-8}$$

and

$$dr = \frac{R}{\tau_R}\,d\tau \quad . \tag{B-9}$$

The Casson relation is expressed as

$$\tau^{1/2} = \tau_o^{1/2} + \left[-\eta \frac{dV_z}{dr}\right]^{1/2} \quad , \tag{B-10}$$

or

$$-\frac{dV_z}{dr} = \frac{(\tau^{1/2} - \tau_o^{1/2})^2}{\eta} \quad \text{for } \tau > \tau_o$$

$$-\frac{dV_z}{dr} = 0 \quad \text{for } \tau < \tau_o \tag{B-11}$$

In general, equation (B-11) can be expressed by the following relation,

$$-\frac{dV_z}{dr} = f(\tau) \quad . \tag{B-12}$$

From equation (B-12), the velocity is given by the integral

$$\int_r^R dV_z = -\int_r^R f(\tau)\,dr \tag{B-13}$$

$$V_z|_R - V_z = -\int_r^R f(\tau)\,dr \tag{B-14}$$

$$V_z = V_z|_R + \int_r^R f(\tau)\,dr \tag{B-15}$$

Substituting the value of dr from equation (B-9) into equation (B-15),

$$V_z = V_z|_R + \int_\tau^{\tau_R} f(\tau)\,d\tau \tag{B-16}$$

The volume rate of flow is given by

$$Q = 2\pi \int_0^R V_z \, r \, dr \quad . \tag{B-17}$$

Substituting equation (B-15) into equation (B-17) yields

$$Q = 2\pi \int_0^R \left[V_z|_R + \int_r^R f(\tau) \frac{R}{\tau_R} \, d\tau \right] r \, dr \tag{B-18}$$

or

$$Q = 2\pi \left[\frac{R^2}{2} V_z|_R + \frac{R}{\tau_R} \int_0^R \left(\int_r^R f(\tau) \, d\tau \right) r \, dr. \right. \tag{B-19}$$

Integrating by parts, equation (B-19) becomes

$$Q = 2\pi \left[\frac{R^2}{2} V_z|_R - \frac{R^3}{2\tau^3} \int_0^R \tau^2 \, f(\tau) \, d\tau \right] \tag{B-20}$$

Using equations (B-8) and (B-9) we get, finally,

$$Q = \pi R^2 \left[V_z|_R - \frac{R}{\tau^3} \int_0^R \tau^2 \, f(\tau) \, d\tau \right] \quad . \tag{B-21}$$

Equations (B-15) and (B-21) give expressions for the velocity and flow for any function $f(\tau)$ and using as boundary conditions

$$V_z = 0 \quad \text{at } r = R$$

and (B-22)

$$\frac{\partial V_z}{\partial r} = 0 \quad \text{at } r = r_o \quad ,$$

where r_o is the radius of the plug-flow region, and is given by (from equation B-6)

$$r_o = \frac{-2}{\Delta p / L} \tau_o \quad . \tag{B-23}$$

Using these boundary conditions and substituting equations (B12) and (B-11) into (B-21) and (B-8), the following relation is found.

$$\frac{4 Q}{\pi R^3} \frac{\gamma_R}{\tau_o} = 1 - (16/7) \gamma^{1/2} + (4/3) \gamma - (1/21) \gamma^4 \tag{B-24}$$

where

$$\gamma = \tau_o / \tau_R = r_o / R \quad .$$

The parameters τ_o and η for the range of flow and tube diameters of practical use in oxygenators were determined, using the data obtained by Dorson and Hershey.[1] Figure 4 (body of report) is a plot of these data for three tube diameters, and the theoretical relation obtained from equation (B-24) using $\tau_o = 0.07$ dynes/cm^2 and $\eta = 0.0283$ poises. These values are reasonable approximations for hematocrits between 31 and 37. The parameter $\bar{U}$ (plotted in fig. 4, body of report) is given by

$$\bar{U} = (\tau_R / 8\eta)[1 + (4/3)\ \gamma - (16/7)\ \gamma^{1/2} - (1/21)\ \gamma^4] \ , \qquad \text{(B-25)}$$

where

$$\bar{U} = Q/2\pi\ R^3 \ . \qquad \text{(B-26)}$$

The velocity profile may be obtained from equations (B-16), (B-11) and (B-12). For $r^* > \gamma$

$$V_z = \frac{R\ \tau_o}{2\ \gamma\ \eta}\left\{1 - (r^*)^2 - (8/3)\ \gamma^{1/2}\ [1 - (r^*)^{3/2}] + 2\gamma(1 - r^*)]\right\} \qquad \text{(B-27)}$$

and for $r^* < \gamma$

$$V_z = \frac{R\ \tau_o}{2\ \gamma\ \eta}\left\{1 + 2\gamma - \gamma^2/3 - (8/3)\ \gamma^{1/2}\right\} \quad . \qquad \text{(B-28)}$$

---

[1]Dorson, W. J. and D. Hershey, Blood Flow Through Long Capillary Tubes, 62nd National Meeting, AIChE. (1967).

APPENDIX C

FLUX THROUGH THE WALL

The third boundary condition can be obtained using the equation of continuity for constant diffusivity to describe the gas flux through the wall.

$$\frac{1}{r}\frac{\partial}{\partial r}\left\{r\frac{\partial C_w}{\partial r}\right\} + \frac{\partial^2 C_w}{\partial Z^2} = 0 \quad , \tag{C-1}$$

where C_w is the equivalent plasma gas concentration for a given gas partial pressure at any point of the wall. Neglecting the second term, which becomes unimportant far from the tube entrance, equation (C-1) becomes

$$\frac{\partial}{\partial r}\left\{r\frac{\partial C_w}{\partial r}\right\} \approx 0 \tag{C-2}$$

and B.C.

$$C_w = C_\infty \text{ at } r = OR$$

$$-D_w \frac{\partial C_w}{\partial r}\Big|_R = n_r\Big|_R \text{ at } r = R$$

where $n_r|_R$ is the radial gas flux at $r = R$.

Integration of equation (C-2) gives

$$r\frac{\partial C_w}{\partial r} = C_1 \quad . \tag{C-3}$$

or

$$D_w\, r\frac{\partial C_w}{\partial r} = C_2 \quad . \tag{C-4}$$

Using the second boundary condition to obtain C_2, equation (C-4) becomes

$$-r\, D_w \frac{\partial C_w}{\partial r} = R\, n_r\Big|_R \quad , \tag{C-5}$$

and the solution of this equation is

$$C_w\Big|_R - C_\infty = \frac{R\, n_r|_R}{D_w} \ell n(OR/R) \tag{C-6}$$

On the other hand, if there is any additional interfacial resistance between the membrane and the blood, the flux through the interfacial film is given by

$$n_r|_R = k\,(C|_R - C_w|_R) \quad , \tag{C-7}$$

where $C|_r$ and $C_w|_r$ are the equivalent gas concentration at the blood face and at the wall, respectively, and k is the mass-transfer coefficient of the additional resistance at the interface between the blood and the membrane (protein deposition, etc).

In the blood face, the flux at the wall is also described by

$$n_r|_R = -D\,\frac{\partial C}{\partial r}|_R \quad . \tag{C-8}$$

Adding equations (C-6) and (C-7), the following expression is obtained.

$$C|_R - C_\infty = n_r|_R\left[1/k + (R/D_w)\,\ln(OR/R)\right] \tag{C-9}$$

and substituting equation (C-9) into equation (C-8) yields

$$D\,\frac{\partial C}{\partial r}|_R = \frac{C_\infty - C|_R}{1/k + (R/D_w)\,\ln(OR/R)} \quad , \tag{C-10}$$

or

$$D\,\frac{\partial}{\partial r^*}[C(1,Z^*)] = F_4\,\frac{D_w}{\ln(OR^*)}\,[C_\infty - C(1,Z^*)] \quad , \tag{C-11}$$

where

$$F_4 = [1 + D_w / k\,R\,\ln(OR^*)]^{-1} \quad . \tag{C-12}$$

APPENDIX D

COMPUTER PROGRAM

To obtain a numerical solution of the transport differential equation, equation (30) in body of report was approximated by the following finite difference equation:

$$\frac{\Delta C}{\Delta Z^*} = \frac{F_2 + N_F F_1^2}{F F_3}\left[\frac{1}{r^*}\left(F_2 + \frac{N_F F_1 (r^*)^{1/2}}{1 + N_F F_1^2}\right)\frac{\Delta C}{\Delta r^*} + \frac{\Delta(\Delta C)}{(\Delta r^*)^2}\right] \qquad \text{(D-1)}$$

Equation (D-1) was rearranged and programmed in the following form.

$$C(r^*+1, Z^*+1) = C(r^*+1, Z^*) + \frac{P}{S}\left\{\frac{FNF}{TK}\left[C(r^*+2, Z^*) - C(r^*+1, Z^*)\right]\right.$$
$$\left. + \left[C(r^*+2, Z^*) - 2\,C(r^*+1, Z^*) + C(r^*, Z^*)\right]\right\} \qquad \text{(D-2)}$$

where the symbol $C(r^*+1, Z^*+1)$ means that the concentration is being evaluated at a point one Δr^* and one ΔZ^* ahead of the point with coordinates (r^*, Z^*), and where

$$P = \Delta Z^*/(\Delta r^*)^2$$

$$S = F F_3/(F_2 + N_F F_1^2)$$

$$FNF = F_2 + N_F F_1 (r^*)^{1/2}/(1 + N_F F_1^2)$$

$$TK = r^*/\Delta r^*$$

The concentration field was divided in 1000 axial and 10 radial zones. Computations done with less axial zones (500 and 700) did not significantly affect the computer results. Also, the results using 20 or 10 radial zones did not differ. The solution of equation (D-2) is executed in the main program and the computation of F_3, percent saturation, and γ are performed in two separate subroutines called COSA and GAMM. The FORTRAN source computer program is given below. The input parameters to the program are listed at the beginning of the source program with a short description of the variable. In the program, when INDX is set to 1, the value of N_F will be computed from the other pertinent variables and the velocity profile computed using the non-Newtonian model. In this case, there is no need to list INDXI or ANF in the NAMELIST. If INDX is set to 2, the computer will read ANF and the velocity will be computed, assuming a parabolic profile. INDXI determines the number of ANF's to be read by the computer, which will repeat the program for each value of ANF. In this case ZMAX should be entered as the largest Z* desired. The values of Q, BETA, TAUO, ETA, NPG, ERG, need not be listed in the NAMELIST since the computer will operate, using the dimensionless variables directly. The value of D should be listed because it is used for the computation of the wall effect (see boundary conditions).

```
$JOB            171603-B,10,2000,VILLAR          BLDG83
$EXECUTE        IBJOB
$IBJOB.         MAP
$IBFTC SSOTP
      REAL NF
      COMMON MP,Q,D,ETA,R,GAMMA,TAUO
      COMMON T,C,CM,E,CF,FC,PS,MP1,B1,B2,B3,CB1,CB2,CB3,CB4,AL1,AL2,PH
      DIMENSION CA(52,6),Z(1005),RS(52),CF(6),E(10),C(52,6),A11(12),
      DIMENSION PS(52,6),PH(52,6),PHA(1005),CAVF(1005),ZD(1005)
      DIMENSION PO2X(52,6),PCO2X(52,6),ANF(10)
      DIMENSION PO2(1005),PCO2(1005),E1(15),FE1(15),DFE1(15),W(12)
      DOUBLE PRECISION CA,C
      NAMELIST/DATA/IMR,IMZ,ZMAX,PHI,CAS,D,Q,R,BETA,CS,CI,CAI,CF,FHSR,
     1TAUO,ETA,OR,DSR,RDSR,NPG,ERG,T,MP,INDX,INDX1,FHSRO,ANF,
     2INDX2,B1,B2,B3,CB1,CB2,CB3,CB4,AL1,AL2
C        IMZ IS THE NO. OF POINTS IN Z DIRECTION
C        IMR IS THE NO. OF POINTS-1 IN R DIRECTION
C        NPG IS THE MAXIMUM NUMBER OF ITERATIONS TO FIND GAMMA
C        ERG IS THE PERCENT ERROR ALLOWED IN GAMMA
C        CI IS THE AVERAGE OXYGEN INPUT PARTIAL PRESSURE IN MMHG
C        CAI IS THE AVERAGE CO2 INPUT PARTIAL PRESSURE IN MMHG
C        CS IS THE O2 PARTIAL PRESSURE AT R=OR IN MMHG
C        PHI IS THE INITIAL VALUE OF PH AT Z=0
C        ZMAX IS THE MAXIMUM VALUE OF Z IN CM
C        OR IS THE OUTSIDE RADIUS IN CM
C        R IS THE INSIDE RADIUS IN CM
C        Q IS THE FLOW PER TUBE IN CC/SEC
C        FHSRO CORREC.FAC. FOR O2 ADDITIONAL INTERFACE RESISTANCE
C        FHSR CORREC.FAC. FOR CO2 ADDITIONAL INTEFACE RESISTANCE
C        D IS THE O2 DIFFUSIVITY IN BLOOD IN CM2/SEC
C        BETA IS THE BLOOD MIXING COEFF. IN CM2
C        ANF IS NF THE DIMENSIONLESS BLOOD MIXING COEFF.
C        INDX=1 COMPUTE NF, =2 READ NF  NF=ANF(N), N=1,INDX1
C        DSR IS THE EQUIVALENT OXYGEN DIFFUSIVITY IN THE WALL IN CM2/SEC
C        RDSR EQUALS DSR(CO2)/DSR
C        T IS THE OXYGEN CONCENTRATION AT 100 PERCENT SATURATION IN M/L
C        TAUO IS THE BLOOD YIELD SHEAR STRESS IN DY/CM2
C        ETA IS THE BLOOD ASYMTOTIC VISCOSITY IN POISES
C        INDX2=2 WRITE PO2,PCO2,PH PROFILES
C        MP IS THE ORDER OF THE POLYNOMIAL REPRESENTING PS UPPER RANGE
C        CF(I) ARE THE COEFF. FOR POLYNOMIAL REPRESENTING PS UPPER RANGE
C        AL1 UPPER LIMIT OF PS MIDDLE RANGE
C        CB1,CB2, COEFF. FOR PS MIDDLE RANGE
C        AL2 UPPER LIMIT OF PS LOWER RANGE
C        CB3, CB4, COEFF. FOR PS LOWER RANGE
      F1(A,B,C)=A/2.+1.-B**2-(8./3.)*SQRT(C)*(1.-B**1.5)+2.*C*(1.-B)
      F2(A,B)=A/2.+1.+2.*B-B**2/3.-(8./3.)*SQRT(B)
    9 READ(5,DATA)
      IF(IMR.EQ.0) GO TO 5555
      IEA=IMR/10
      INC=0
      KK=1
      NF=ANF(1)
      MP1=MP+1
      PO2(1)=CI
      PCO2(1)=CAI
      WRITE(6,204)
  204 FORMAT(51H1OXYGEN TRANSFER TO BLOOD FLOWING STEADILY IN TUBES//)
      WRITE(6,205)
  205 FORMAT(/17X3HIMR,17X3HIMZ,18X2HMP,17X3HNPG,16X4HINDX,15X5HINDX1//)
```

```
      WRITE(6,206) IMR,IMZ,MP,NPG,INDX,INDX1
      WRITE(6,207)
  207 FORMAT(//18X2HCS,18X2HCI,16X4HZMAX,17X3HPHI,17X3HCAS,17X3HCAI//)
      WRITE(6,208) CS,CI,ZMAX,PHI,CAS,CAI
      WRITE(6,212)
  212 FORMAT(//19X1HD,19X1HQ,19X1HR,16X4HRDSR,19X1HT,16X4HBETA//)
      WRITE(6,208) D,Q,R,RDSR,T,BETA
      WRITE(6,213)
  213 FORMAT(//16X4HTAUO,17X3HETA,17X3HERG,18X2HOR,17X3HDSR//)
      WRITE(6,208) TAUO,ETA,,ERG,OR,DSR
      WRITE(6,2090)
 2090 FORMAT(//15X5HINDX2,16X4HFHSR,15X5HFHSRO,17X3HDNF,18X2HNF//)
      WRITE(6,2210) INDX2,FHSR,FHSRO,DNF,NF
 2210 FORMAT(I20,4F20.4)
      WRITE(6,2091)
 2091 FORMAT(//18X2HB1,18X2HB2,18X2HB3,17X3HCB1,17X3HCB2,17X3HCB3//)
      WRITE(6,208) B1,B2,B3,CB1,CB2,CB3
      WRITE(6,2092)
 2092 FORMAT(//17X3HCB4,17X3HAL1,17X3HAL2//)
      WRITE(6,208) CB4,AL1,AL2
      WRITE(6,209)
      WRITE(6,208) (CF(I),I=1,MP1)
  209 FORMAT(///,17X3HCF1,17X3HCF2,17X3HCF3,17X3HCF4,17X3HCF5,17X3HCF6/)
  206 FORMAT(6I20)
  208 FORMAT(5E20.8)
  221 FORMAT(5E20.8)
      CM=.4643E-3
      CS=CS/7.E+5
      CAS=CAS/3.59E4
      CAI=CAI/3.59E4
      CI=CI/7.E+5
  444 CONST=4.
      IF(INDX.EQ.1) GO TO 33
      GAMMA=0.0
      ZSMAX=ZMAX
      GO TO 34
   33 CALL GAMM(NPG,ERG,IERR)
      IF(IERR.NE.0) GO TO 400
      CONST=3.14159*R**3*TAUO/(Q*GAMMA*ETA)
      NF=TAUO*BETA/(GAMMA*ETA*D)
      ZSMAX=ZMAX/(TAUO*R**3/(GAMMA*2.*ETA*D))
   34 CPH=CAI*10.**(PHI-6.11)
      MR=IMR+1
      DR=1./FLOAT(IMR)
      DZ=ZSMAX/FLOAT(IMZ-1)
      P=DZ/DR**2
      RS(1)=0
      DO 3 I=2,MR
    3 RS(I)=RS(I-1)+DR
      Z(1)=0
      ZD(1)=0
      DO 10 J=2,IMZ
      Z(J)=Z(J-1)+DZ
   10 ZD(J)=ZMAX*Z(J)/ZSMAX
         SET ALL CONCENTRATIONS AT Z=ZO FOR ALL R TO INITIAL VALUE
      IK=0
      IMZ1=IMZ
      DW=D*(1.+NF)*(1.-SQRT(GAMMA))**2
      G=DW*ALOG(OR/R)*FHSRO/(DSR*DR)
      GA=0.9833*G*FHSR/(RDSR*FHSRO)
```

```
      DO 1 I=1,MR
      C(I,1)=CI
      CA(I,1)=CAI
    1 PH(I,1)=PHI
      PHA(1)=PHI
      MT=IMR-1
      IM1=IMZ-1
C         SOLVE PARTIAL DIFFERENTIAL EQUATION FOR CONCENTRATION
      JJ=0
  111 IF(INDX2.NE.2) GO TO 1111
      IK=IK+1
      DO 1122 I=1,MR
      PO2X(I,1)=C(I,1)*7.E5
 1122 PCO2X(I,1)=CA(I,1)*3.59E4
      IF(IK.NE.1) GO TO 1113
      WRITE(6,1112)
 1112 FORMAT(1H1,45X2HR*//6X2HZ*,10X3H0.0,4X3H0.1,4X3H0.2,4X3H0.3,4X3H0.
     24,4X3H0.5,4X3H0.6,4X3H0.7,4X3H0.8,4X3H0.9,4X3H1.0//)
 1113 WRITE(6,1114) Z(JJ),(PO2X(IN,1),IN=1,MR,IEA)
 1114 FORMAT(2X,F6.3,2X4HPO2=,11F7.2)
      WRITE(6,1115) (PCO2X(IN,1),IN=1,MR,IEA)
 1115 FORMAT(9X5HPCO2=,11F7.2)
      WRITE(6,1116) (PH(IN,1),IN=1,MR,IEA)
 1116 FORMAT(11X3HPH=,11F7.3//)
 1111 DO 5 J=1,5
      JJ=JJ+1
      DO 4 K=1,MT
      TK=K
      TK=K
      KP1=K+1
      CALL COSA(KP1,J)
      IF(RS(K+1).GE.GAMMA) GO TO 79
      F=F2(ALPHA,GAMMA)
      S=(FC+1.)*F
      SA=10.*F/0.9833
      GO TO 80
   79 F=F1(ALPHA,RS(K+1),GAMMA)
      S=(FC+1.)*F/(1.+NF*(SQRT(RS(K+1))-SQRT(GAMMA))**2)
      SA=10.*F/(0.9833+NF*(SQRT(RS(K+1))-SQRT(GAMMA))**2)
   80 FNF=1.+(NF*(RS(K+1)-SQRT(RS(K+1))*SQRT(GAMMA)))/(1.+NF*(SQRT(RS(K+
     1 1))-SQRT(GAMMA))**2)
      FNFA=0.9833+(NF*(RS(K+1)-SQRT(RS(K+1))*SQRT(GAMMA)))/(0.9833+NF*
     1 (SQRT(RS(K+1))-SQRT(GAMMA))**2)
      C(K+1,J+1)=C(K+1,J)+(P/S)*((C(K+2,J)-2.*C(K+1,J)+C(K,J))+
     1    (C(K+2,J)-C(K+1,J))*FNF/TK)
      IF(C(K+1,J+1).LT.C(K+1,J)) C(K+1,J+1)=C(K+1,J)
      IF(C(K+1,J+1).LE.CS) GO TO 4
      C(K+1,J+1)=CS
    4 CA(K+1,J+1)=CA(K+1,J)+(P/SA)*((CA(K+2,J)-2.*CA(K+1,J)+CA(K,J))+
     1    (CA(K+2,J)-CA(K+1,J))*FNFA/TK)
C         BOUNDARY CONDITION-DC/DZ=0 FOR R=0
      C(1,J+1)=C(2,J+1)
      CA(1,J+1)=CA(2,J+1)
C         COMPUTE CONCENTRATION AT THE WALL
      C(IMR+1,J+1)=(CS+G*C(IMR,J+1))/(1.+G)
      IF(C(IMR+1,J+1).LE.CS) GO TO 85
      C(IMR+1,J+1)=CS
   85 CA(IMR+1,J+1)=(CAS+GA*CA(IMR,J+1))/(1.+GA)
C         PS AT THE BOUNDARIES
      PS(1,J)=PS(2,J)
```

```
      IMR1=IMR+1
      CALL COSA(IMR1,J)
      DO 6 K=1,MR
    6 PH(K,J+1)=6.11+ALOG10(CPH/CA(K,J+1))
      CAAVF1=0
      CAVF1=0
      DO 350 I=1,IMR
      RI=(RS(I)+RS(I+1))/2.
      IF(RI.GE.GAMMA) F=F1(ALPHA,RI,GAMMA)
      IF(RI.LE.GAMMA) F=F2(ALPHA,GAMMA)
      CARI=(CA(I,J)+CA(I+1,J))/2.
      CRI=(PS(I,J)+PS(I+1,J))/2.
      CAAVF1=CAAVF1+RI    *F*CARI
  350 CAVF1=CAVF1+RI    *F*CRI
      CAAVF1=CAAVF1*CONST*DR
      PHA(JJ)=6.11+ALOG10(CPH/CAAVF1)
      CAVF(JJ)=CAVF1*CONST*DR
      IF(INC.EQ.1) GO TO 96
      IF(CAVF(JJ).GE.1000.) INC=1
      IF(CAVF(JJ).GE.100.) GO TO 3500
      IF(CAVF(JJ).LT.58.5) GO TO 3512
      IF(CAVF(JJ).LE.95.0) GO TO 345
      W(1)=SQRT(0.076415E-8/ALOG(100.4/CAVF(JJ)))
      GO TO 35
  345 W(1)=SQRT(0.10409E-8/ALOG(102.57/CAVF(JJ)))
   35 I=1
   37 E(1)=1./W(I)
      DO 460 L=2,MP1
  460 E(L)=E(L-1)*E(1)
      A11(I)=CF(2)*E(1)
      DO 430 L=2,MP
  430 A11(I)=A11(I)+CF(L+1)*E(L)
      A11(I)=EXP(A11(I))*CF(1)
      DA1=(CAVF(JJ)-A11(I))/CAVF(JJ)
      IF(ABS(DA1).LE.0.002) GO TO 450
      IF(I.GT.1) GO TO 482
      SIG=A11(I)-CAVF(JJ)
      SIG=SIG/ABS(SIG)
      W(I+1)=W(I)+SIG*1.43E-6
      GO TO 481
  482 V2=ALOG(A11(I-1)/A11(I))
      V2=V2/(W(I-1)**(-2)-W(I)**(-2))
      V1=A11(I)/EXP(V2*W(I)**(-2))
      W(I+1)=SQRT(-V2/ALOG(V1/CAVF(JJ)))
      IF(I.GT.10) GO TO 38
  481 I=I+1
      GO TO 37
 3512 IF(CAVF(JJ).LT.23.5) GO TO 3513
      W(1)=(CAVF(JJ)+11.2)/CB1
      GO TO 450
 3513 SQ=SQRT(CB3**2+4.*CB4*CAVF(JJ))
      W(1)=(SQ-CB3)/(2.*CB4)
  450 PO2(JJ)=W(I)*7.E+5/(B1-B2*PHA(JJ)+B3*PHA(JJ)**2)
      GO TO 39
   38 PO2(JJ)=1000.
   39 PCO2(JJ)=CAAVF1*3.59E+4
      IF(JJ.GT.IMZ) GO TO 3500
    5 CONTINUE
      DO 2 I=1,MR
      C(I,1)=C(I,J+1)
```

```
      CA(I,1)=CA(I,J+1)
    2 PH(I,1)=PH(I,J+1)
      GO TO 111
   00 IMZ1=JJ-1
   60 WRITE(6,420) NF
   20 FORMAT(1H1,3HNF=,E20.8//)
      IF(INDX.EQ.2) GO TO 93
      WRITE(6,423)
   23 FORMAT(14X6HLENGTH,7X13HDIMENSIONLESS,13X7HPERCENT,13X7HAVERAGE,
     1 17X3HPO2,16X4HPCO2)
      WRITE(6,424)
   24 FORMAT(18X2HCM,14X6HLENGTH,10X10HSATURATION,18X2HPH,
     1 16X4HMMHG,16X4HMMHG)
      WRITE(6,208) (ZD(JJ),Z(JJ),CAVF(JJ),PHA(JJ),PO2(JJ),
     1 PCO2(JJ),JJ=1,IMZ1,10)
      GO TO 95
   93 WRITE(6,421)
   21 FORMAT(7X13HDIMENSIONLESS,13X7HPERCENT,13X7HAVERAGE,
     1 17X3HPO2,16X4HPCO2)
      WRITE(6,422)
   22 FORMAT(14X6HLENGTH,10X10HSATURATION,18X2HPH,16X4HMMHG,16X4HMMHG/)
      WRITE(6,221) (Z(JJ),CAVF(JJ),PHA(JJ),PO2(JJ),PCO2(JJ),
     1JJ=1,IMZ1,10)
      IF(INDX.EQ.1) GO TO 96
      GO TO 95
  )00 WRITE(6,233)
  233 FORMAT(39H GAMMA DID NOT CONVERGE TO PROPER VALUE//)
      GO TO 95
   95 IF(INDX1.EQ.0) GO TO 96
      IF(KK.GE.INDX1) GO TO 96
      KK=KK+1
      NF=ANF(KK)
      ZMAX=1./NF+0.07
      IF(ZMAX.GT.0.14) ZMAX=0.14
      GO TO 444
   96 CS=CS*7.E+5
      CAS=CAS*3.59E4
      CAI=CAI*3.59E4
      CI=CI*7.E+5
      GO TO 9
 5555 STOP
      END
$IBFTC GAMM1
      SUBROUTINE GAMM(NPG,ERG,IERR)
      COMMON MP,Q,D,ETA,R,GAMMA,TAUD
      DIMENSION GAM(50)
      IERR=0
      A=4.*Q*ETA/(3.14159*R**3*TAUD)
      GAM(1)=1./(2.*A)
      I=1
   10 FG=1.-(16./7.)*SQRT(GAM(I))+((4./3.)-A)*GAM(I)-GAM(I)**4/21.
      DFG=-(8./7.)/SQRT(GAM(I))+4./3.-A-(4./21.)*GAM(I)**3
      GAM(I+1)=GAM(I)-FG/DFG
      IF(ABS((GAM(I+1)-GAM(I))/GAM(I+1)).LE.ERG) GO TO 100
      IF(GAM(I+1).LT.0.) GO TO 30
      IF(I.GE.NPG) GO TO 200
   15 I=I+1
      GO TO 10
  100 IF(GAM(I+1).LT.0.0)GAM(I+1)=0.0
      IF(GAM(I+1).GT.1.0)GAM(I+1)=1.0
```

```
      GAMMA=GAM(I+1)
      RETURN
   30 J=1
   31 GAM(I+1)=GAM(I)-(FG/DFG)*.5**J
      IF(GAM(I+1).GE.0.) GO TO 15
      J=J+1
      GO TO 31
  200 IERR=1
      RETURN
      END
$IBFTC COSA1
      SUBROUTINE COSA(JO,JU)
      COMMON MP,Q,D,ETA,R,GAMMA,TAUO
      COMMON T,C,CM,E,CF,FC,PS,MP1,B1,B2,B3,CB1,CB2,CB3,CB4,AL1,AL2,PH
      DIMENSION C(52,6),E(10),CF(6),PS(52,6),PH(52,6)
      DOUBLE PRECISION C
      FPH=B1-B2*PH(JO,JU)+B3*PH(JO,JU)**2
      W=FPH*C(JO,JU)
      IF(W.LT.AL1) GO TO 88
      IF(W.GE.CM) GO TO 77
      E(1)=1./W
      DO 16 L=2,MP1
   16 E(L)=E(L-1)*E(1)
      A1=CF(2)*E(1)
      DO 13 L=2,MP
   13 A1=A1+CF(L+1)*E(L)
      A1=EXP(A1)
      A2=CF(2)*E(2)
      DO 14 L=3,MP1
      Q1=L-1
   14 A2=A2+CF(L)*Q1*E(L)
      FC=-(T/100.)*CF(1)*A2*A1*FPH
      PS(JO,JJ)=CF(1)*A1
      GO TO 78
   77 FC=0.0
      CM1=CM/FPH
      PS(JO,JJ)=100.*(1.+(C(JO,JU)-CM1)/T)
      GO TO 78
   88 IF(W.LT.AL2) GO TO 46
      PS(JO,JJ)=CB1*W-CB2
      FC=T*CB1*FPH/100.
      GO TO 78
   46 PS(JO,JJ)=CB3*W+CB4*W**2
      FC=T*(CB3+CB4*2.*W)*FPH/100.
   78 RETURN
      END
```

NOMENCLATURE

c_m - Gas solubility in the membrane

c_p - Gas solubility in the plasma

C - Concentration of the gas in the plasma

C_o - Initial concentration of the gas in the plasma

C_w - Equivalent concentration of the gas in the wall

C_∞ - Equivalent concentration of the gas in the atmosphere outside the tube

D - Effective diffusivity of the gas in whole blood

D_m - Diffusivity of the gas in the membrane

D_o - Ordinary diffusivity of the gas in whole blood

D_p - Ordinary diffusivity of the gas in plasma

D_{rbc} - Diffusivity of the gas in the red cells

D_{rot} - Rotation-induced diffusivity of the gas in whole blood

D_w - Equivalent diffusivity of the gas in the wall

F - $1 - \gamma^2 - (8/3)\,\gamma^{1/2}\,[1 - (r^*)^{3/2}] + 2\,\gamma\,(1 - r^*)$, for $r^* > \gamma$

F - $1 - 2\,\gamma - (1/3)\,\gamma^2 - (8/3)\,\gamma^{1/2}$, for $r^* < \gamma$

F_1 - $(r^*)^{1/2} - \gamma^{1/2}$, for $r^* > \gamma$

F_1 - 0 , for $r^* < \gamma$

F_2 - 1.0 , for oxygen

F_2 - 0.9833 , for carbon dioxide

F_3 - $1 + ds/dC$

F_4 - $(1 + D_w / k\,R\,\ln OR^*)^{-1}$

g% - Grams per 100 cc of blood

H - Hematocrit, volumetric percent of red cells in whole blood

NOMENCLATURE (Cont'd)

ID	-	Inside diameter
K_{pH}	-	pH mapping factor, equation (A-11)
L	-	Length of the tube
n_r	-	Radial flux
n_{rot}	-	Rotation-induced flux
N_F	-	Dimensionless blood mixing coefficient
OD	-	Outside diameter
OR	-	Outside radius
OR*	-	Dimensionless outside radius
p	-	Pressure
pCO_2	-	Partial pressure of carbon dioxide
pH	-	$-\log [H_3O^+]$
pO_2	-	Partial pressure of oxygen
P_m	-	Permeability of the wall
PS	-	Oxygen percent of saturation
PS_v	-	Oxygen percent of saturation of the venous blood
Q	-	Blood flow
r	-	Radial distance
r*	-	Dimensionless radial distance
r_o	-	Radius of the plug-flow region
R	-	Inside radius
s	-	Concentration of the gas stored in the sinks
S	-	Apparent reaction rate
T	-	Oxygen concentration in blood at 100-percent saturation

V_z - Axial velocity

V_θ - Tangential velocity

X - Fricke's geometrical parameter

Z - Axial distance

Z* - Dimensionless axial distance

Z** - $(1 - PS_v/100)\ (\pi\ D_o\ Z/\ 2\ Q)$

Greek

β - Blood mixing coefficient

γ - Dimensionless radius of the plug-flow region

δ - Erythrocyte diameter

ΔC - Concentration increment

Δp - Differential pressure across the tube

ΔPS - Increment in the oxygen percent of saturation from the venous saturation value

ΔPS^* - Generalized increment in the oxygen percent of saturation from the venous saturation value

Δr - Increment in the radial direction

ΔZ - Increment in the axial direction

η - Viscosity of the blood

π - 3.1416

ρ - Density of the blood

τ - Shear stress

τ_o - Yield shear stress

τ_R - Shear stress at the wall

ϕ - Correction factor, equation (26)

NOMENCLATURE (Cont'd)

Special

$\|_r$	-	At position r
$\|_{r+\Delta r}$	-	At position r + Δr
$\|_R$	-	At r = R
$\|_z$	-	At position Z
$\|_{z+\Delta z}$	-	At position Z + ΔZ
[ ]	-	Concentration of a chemical specie

Chemical

CO_2	-	Carbon dioxide
HCO_3^-	-	Bicarbonate ion
H_2O	-	Water
H_3O^+	-	Hydronium ion
O_2	-	Oxygen

UNCLASSIFIED

Security Classification

DOCUMENT CONTROL DATA - R & D

(Security classification of title, body of abstract and indexing annotation must be entered when the overall report is classified)

1. ORIGINATING ACTIVITY *(Corporate author)*

Harry Diamond Laboratories
Washington, D. C. 20438

2a. REPORT SECURITY CLASSIFICATION

UNCLASSIFIED

2b. GROUP

3. REPORT TITLE

MATHEMATICAL MODELING OF RESPIRATORY GAS EXCHANGE IN CAPILLARY TUBE OXYGENATORS WITH STEADY BLOOD FLOW

4. DESCRIPTIVE NOTES *(Type of report and inclusive dates)*

5. AUTHOR(S) *(First name, middle initial, last name)*

Fernando Villarroel

6. REPORT DATE	7a. TOTAL NO. OF PAGES	7b. NO. OF REFS
August 1970	76	31

8a. CONTRACT OR GRANT NO.	9a. ORIGINATOR'S REPORT NUMBER(S)
b. PROJECT NO. DA-3A062110A816.10	HDL-TM-70-18
c. AMCMS Code: 5910.21.63232	9b. OTHER REPORT NO(S) *(Any other numbers that may be assigned this report)*
d. HDL Proj: 31000	

10. DISTRIBUTION STATEMENT

This document has been approved for public release and sale; its distribution is unlimited.

11. SUPPLEMENTARY NOTES	12. SPONSORING MILITARY ACTIVITY
	Surgical Directorate of the U. S. Army Medical R & D Command

13. ABSTRACT

A mathematical model for the transport of oxygen and carbon dioxide to blood flowing in semipermeable tubes under steady-flow conditions is presented. The model considers the membrane resistance to gas transport and allows for an additional interfacial resistance (protein deposition, etc). The possibility of gas transport augmentation due to rotation of erythrocytes in the velocity field is included in the model; however, no evidence of this augmentation was found in the flow range in which the model was compared with experimental data. The partial differential equation for the gas transport was solved numerically using a digital computer. Simultaneous solutions for oxygen and carbon dioxide were obtained, and the pH was computed for any point in the tube. Comparison of experimental data obtained by the author and other investigators with the curves predicted by the model shows excellent agreement. The numerical solution of the transport equation yields the bulk average values of pH, carbon dioxide partial pressure, and oxygen saturation, as well as the internal value of these parameters as a function of tube length and radius. A simple steady flow design equation, which is a reasonable approximation of the computer results for a wide range of venous blood conditions, is presented.

DD FORM 1 NOV 65 1473 REPLACES DD FORM 1473, 1 JAN 64, WHICH IS OBSOLETE FOR ARMY USE.

UNCLASSIFIED

Security Classification

14. KEY WORDS	LINK A		LINK B		LINK C	
	ROLE	WT	ROLE	WT	ROLE	WT
Mass transfer	8	2				
Oxygenators	8	3				
Mathematical modeling	8	2				
Blood	8	2				
Capillary tubes	8	1				
Carbon dioxide removal from blood	8	3				
Steady blood flow	8	2				